JOURNAL OF VIROLOGY, Jan. 2005, p. 1191–1206 Vol. 79, No. 2
0022-538X/05/$08.00+0 doi:10.1128/JVI.79.2.1191–1206.2005

Kaposi's Sarcoma-Associated Herpesvirus Modulates Microtubule Dynamics via RhoA-GTP-Diaphanous 2 Signaling and Utilizes the Dynein Motors To Deliver Its DNA to the Nucleus

Pramod P. Naranatt, Harinivas H. Krishnan, Marilyn S. Smith, and Bala Chandran*

Department of Microbiology, Molecular Genetics and Immunology, The University of Kansas Medical Center, Kansas City, Kansas

Received 6 February 2004/Accepted 3 September 2004

Human herpesvirus 8 (HHV-8; also called Kaposi's sarcoma-associated herpesvirus), which is implicated in the pathogenesis of Kaposi's sarcoma (KS) and lymphoproliferative disorders, infects a variety of target cells both in vivo and in vitro. HHV-8 binds to several in vitro target cells via cell surface heparan sulfate and utilizes the α3β1 integrin as one of its entry receptors. Interactions with cell surface molecules induce the activation of host cell signaling cascades and cytoskeletal changes (P. P. Naranatt, S. M. Akula, C. A. Zien, H. H. Krishnan, and B. Chandran, J. Virol. 77:1524–1539, 2003). However, the mechanism by which the HHV-8-induced signaling pathway facilitates the complex events associated with the internalization and nuclear trafficking of internalized viral DNA is as yet undefined. Here we examined the role of HHV-8-induced cytoskeletal dynamics in the infectious process and their interlinkage with signaling pathways. The depolymerization of microtubules did not affect HHV-8 binding and internalization, but it inhibited the nuclear delivery of viral DNA and infection. In contrast, the depolymerization of actin microfilaments did not have any effect on virus binding, entry, nuclear delivery, or infection. Early during infection, HHV-8 induced the acetylation of microtubules and the activation of the RhoA and Rac1 GTPases. The inactivation of Rho GTPases by *Clostridium difficile* toxin B significantly reduced microtubular acetylation and the delivery of viral DNA to the nucleus. In contrast, the activation of Rho GTPases by *Escherichia coli* cytotoxic necrotizing factor significantly augmented the nuclear delivery of viral DNA. Among the Rho GTPase-induced downstream effector molecules known to stabilize the microtubules, the activation of RhoA-GTP-dependent diaphanous 2 was observed, with no significant activation in the Rac- and Cdc42-dependent PAK1/2 and stathmin molecules. The nuclear delivery of viral DNA increased in cells expressing a constitutively active RhoA mutant and decreased in cells expressing a dominant-negative mutant of RhoA. HHV-8 capsids colocalized with the microtubules, as observed by confocal microscopic examination, and the colocalization was abolished by the destabilization of microtubules with nocodazole and by the phosphatidylinositol 3-kinase inhibitor affecting the Rho GTPases. These results suggest that HHV-8 induces Rho GTPases, and in doing so, modulates microtubules and promotes the trafficking of viral capsids and the establishment of infection. This is the first demonstration of virus-induced host cell signaling pathways in the modulation of microtubule dynamics and in the trafficking of viral DNA to the infected cell nucleus. These results further support our hypothesis that HHV-8 manipulates the host cell signaling pathway to create an appropriate intracellular environment that is conducive to the establishment of a successful infection.

The gamma-2 human herpesvirus 8 (HHV-8), or Kaposi's sarcoma-associated herpes virus (KSHV), genome was first identified in biopsies of KS, an AIDS-defining neoplasm of human immunodeficiency virus (HIV)-infected patients (16). Several lines of evidence point to a central role of HHV-8 in the pathogenesis of KS and of two B-cell proliferative disorders, primary effusion lymphoma (or body-cavity-based B-cell lymphomas [BCBL]) and multicentric Castleman's disease (58). HHV-8 DNA and transcripts have been identified in vivo in KS spindle and endothelial cells, keratinocytes, prostate epithelial cells, B cells, and macrophages (9, 58). In vitro, HHV-8 has been shown to infect many types of human cells, such as B, epithelial, endothelial, and foreskin fibroblast (HFF) cells and keratinocytes (11, 57, 66). HHV-8 can also infect animal cells, such as mouse embryonic fibroblasts (11, 50), owl monkey kidney cells, CV-1 cells, and baby hamster kidney (BHK-21) cells (11, 57). HHV-8 enters human fibroblast, B (BJAB), and embryonic kidney (293) cells by endocytosis (3, 6, 36), and this uptake is severely attenuated in cells that are pretreated with inhibitors affecting endosomal functions (6, 36).

HHV-8 utilizes the ubiquitous cell surface heparan sulfate (HS) to bind several in vitro target cells (3), and this interaction is mediated by the virion envelope-associated glycoproteins gB and gpK8.1A (4, 67). HHV-8 gB also interacts with the host cell surface α3β1 integrin and utilizes the α3β1 integrin as one of its cellular receptors (5). Using a KSHV ORF50-dependent reporter 293-T cell line, Inoue et al. (36) reported the inability of soluble α3β1 integrin and RGD peptides to block the infectivity of HHV-8. However, in their study the virus was centrifuged with cells in the presence of Polybrene, which may account for the apparent discrepancy. Polybrene is

* Corresponding author. Mailing address: Department of Microbiology, Molecular Genetics and Immunology, Mail Stop 3029, The University of Kansas Medical Center, 3901 Rainbow Blvd., Kansas City, KS 66160. Phone: (913) 588-7043. Fax: (913) 588-7295. E-mail: bchandra@kumc.edu.

a positively charged cation which can complex with the virus envelope and bypass the need for receptors. This property of Polybrene is the basis for its use to increase the infectivity of many viruses and to deliver nucleic acids for gene therapy. The nature of the other receptor(s) recognized by HHV-8 and the glycoproteins involved need to be evaluated further.

The precise mechanisms of HHV-8 entry, transport of virus capsids in the cytoplasm, delivery of viral DNA to the nucleus, and initiation of infection have not been fully explored. To establish a successful infection, viruses must cross the plasma membrane and target their genome and accessory proteins to the correct organelle, where gene transcription, nucleic acid replication, and viral maturation can take place. After cell membrane penetration, viruses encounter the formidable barrier of the cytoplasm, which is packed with organelles, solutes, and a complex cytoskeletal network consisting of microtubules (MTs), actin microfilaments (MFs), and intermediate filaments (IFs), all of which restrict the free diffusion of macromolecular complexes larger than 500 kDa or 50 nm (59, 63). Several viruses overcome these barriers by using the host cell macromolecule transport mechanism to move within the cell (14). The movement of large cargo, including membrane organelles, involves either the MF or MT network. Adenoviruses use the microtubules to reach the target cell nucleus, and the disassembly of viral capsids near the nuclear pores allows the viral DNA to enter the nucleus (25, 61, 62, 64, 69). The MT network has also been shown to be utilized by herpes simplex virus type 1 (HSV-1) to transport its capsid (31, 44, 61, 69) and by HIV type 1 (HIV-1) to transport its subviral particle containing the newly synthesized preinitiation complex cDNA (47, 69).

An HHV-8–integrin interaction results in the activation of integrin-associated focal adhesion kinase (FAK) and phosphatidylinositol 3-kinase (PI-3K) (50). Two of the hallmarks of an integrin interaction with ligands are the reorganization and remodeling of the cytoskeleton, which are controlled by the Rho, Rac, and Cdc42 GTPases (13). Immediately after infection, HHV-8 induces the rapid polymerization of actin in the target cells, leading to an increase in the F-actin content, an accumulation of stress fibers, the formation of filopodial extensions, and cellular ruffling (50). These morphological changes are also induced by HHV-8 gB and are inhibited by PI-3K inhibitors (60). These data suggest that HHV-8 modulates the cytoskeletal network dynamics in a PI-3K- and Rho GTPase-dependent manner (50, 60). To investigate the role of HHV-8-induced cytoskeletal dynamics in the infectious process, we analyzed the events promoting the nuclear trafficking of internalized HHV-8. In this report, we demonstrate that MTs are vital for the trafficking of viral DNA to the infected cell nucleus. Antibodies against the HHV-8 capsid showed that the viral capsid colocalizes with the MTs near the vicinity of the nucleus, and the inhibition of MT polymerization and Rho GTPases abolished the migration of capsids in the cytoplasm. Our studies also show that HHV-8 utilizes the MT-dependent dynein motor for the transport of its DNA towards the nucleus. These results demonstrate that HHV-8 manipulates the host cell signaling pathways to promote the trafficking of its capsid and to establish a successful infection.

MATERIALS AND METHODS

Cells and plasmids. Human fibroblast cells (HFF; Clonetics, Walkersville, Md.), human dermal microvascular endothelial cells (CC-2543; Clonetics), human embryonic kidney cells (293), CV-1 cells, HHV-8-carrying human B cells (BCBL-1), recombinant green fluorescent protein–HHV-8 (GFP–HHV-8–γKSHV.150)-carrying BCBL-1 cells (GFP–BCBL-1) (66), and BJAB cells (HHV-8- and Epstein-Barr virus-negative human B cells) were grown per standard procedures established in the laboratory (3–6, 50). A Myc-tagged p50/dynamitin construct (30) was a kind gift from Richard Vallee, Department of Pathology, Columbia University, New York, N.Y. Transfections of 293 and CV-1 cells with 3 μg of p50/dynamitin were performed by the use of Lipofectamine 2000 (Invitrogen, Carlsbad, Calif.) as described previously (49, 50).

Transfection and GTP-loading assay. 293 cells were transfected with the wild type (wt) and with dominant-negative (T19N) and constitutively active (G14V) mutants of RhoA plasmids obtained from the Guthrie cDNA resource center (http://www.cdna.org). Plasmid DNA (2.5 μg) was used for transfections, and G418 selection was performed to establish stable cell lines carrying each mutant. Each cell line carrying either a wt or mutant Rho plasmid was first characterized by a GTP-loading assay to confirm its phenotype. Lysates of each cell line were made by using RIPA lysis buffer containing protease inhibitors and were normalized to contain equal protein concentrations before the addition of 5 μl of GTPγS (Upstate Biotechnology, Charlottesville, Va.). The mixture was incubated at 30°C for 15 min with agitation (GTP loading), and the reaction was terminated by the addition of $MgCl_2$ to a concentration of 50 μM. The amounts of activated Rho (Rho-GTP) in the reaction mixtures were detected by affinity precipitation (4°C for 45 min) using rhotekin-GST beads. Bound RhoA proteins were resolved by sodium dodecyl sulfate–12% polyacrylamide gel electrophoresis (SDS–12% PAGE) and immunoblotted with rabbit polyclonal antibodies against RhoA. These characterized cells were used to examine the role of Rho in HHV-8 nuclear trafficking.

Virus. HHV-8 was purified from BCBL cells according to previously described methods (3, 48, 50), and the purity of the preparation was assessed by guidelines established in our laboratory (3, 48, 50). HHV-8 DNA was extracted from the virus, and the copy numbers were quantified by real-time DNA PCR using primers amplifying the HHV-8 ORF73 gene (43).

Antibodies, toxins, and reagents. Polyclonal rabbit antibodies to Cdc42, Rac1, RhoA, and diaphanous 2 (Dia2) and a monoclonal (MAb) antibody against the c-*myc* tag were obtained from Santa Cruz Biotechnology, Santa Cruz, Calif. A MAb against GFP was obtained from Covance Research Products, Berkeley, Calif. MAbs against β-actin, α-tubulin, and an acetylated form of α-tubulin, tetradecanoyl phorbol acetate, and lysophosphatidic acid (LPA) were obtained from Sigma. Rabbit antibodies against human PAK-1 (total) and phospho-PAK1/2 (Ser 199/204 and Ser 192/197) were obtained from Cell Signaling Technology, Beverly, Mass. Anti-rabbit and anti-mouse antibodies linked to horseradish peroxidase, fluorescein isothiocyanate, Alexa 488, and Alexa 594 were purchased from KPL Inc., Gaithersburg, Md., or Molecular Probes, Eugene, Oreg. The cytoskeletal depolymerizing agents nocodazole, cytochalasin D (cyto D), latrunculin A (lat A), *N*-deacetyl-*N*-methylcolchicine (Colcemid), and paclitaxel (Taxol) were purchased from Sigma. *Clostridium difficile* toxin B (CdTxB) and a MAb against lamin B were obtained from Calbiochem, La Jolla, Calif. Cytotoxic necrotizing factor 1 (CNF-1) from *Escherichia coli* (2) was a kind gift from Gudula Schmidt, Universitat Freiburg, Freiburg, Germany. Rabbit polyclonal antibodies detecting total stathmin and phosphorylated stathmin (Ser 16) were kind gifts from Andre Sobel, INSERM U440, Institut du Fer a Moulin, Paris, France (27).

GFP–HHV-8 infection and HHV-8 binding assay. The effects of inhibitors on HHV-8 infection were measured by using GFP–HHV-8 (rKSHV.152) per previously described procedures (3, 49, 50). [^{3}H]thymidine-labeled HHV-8 was used to assess the effects of various inhibitors on HHV-8 binding according to previously described procedures (3).

Real-time DNA and RT-PCR. Real-time DNA PCR and real-time reverse transcription-PCR (RT-PCR) were performed to quantify the internalized viral DNA and to monitor HHV-8 ORF73 mRNA expression, respectively (43).

HHV-8 DNA nuclear delivery assay. To monitor the delivery of HHV-8 DNA to HFF cell nuclei, we prepared pure nuclear fractions by use of a Nuclei EZ isolation kit (Sigma) according to the manufacturer's recommendations. Briefly, cells infected with HHV-8 were collected at different times postinfection (p.i.), washed, treated with trypsin-EDTA (0.25% trypsin and 5 mM EDTA) to remove noninternalized virus, and lysed on ice for 5 min with a mild lysis buffer (Sigma), and the nuclei were concentrated by centrifugation at 500 × *g* for 5 min. Cytoskeletal components loosely bound to the nuclei were removed from the nuclear pellet by a repeat of the lysis and centrifugation procedures. The nuclei

from one 25-cm^2 flask were resuspended in nucleus homogenization buffer (250 mM sucrose, 5 mM $MgCl_2 \cdot 6H_2O$, 25 mM KCl, 20 mM Tricine-KOH, 7.8), and 60% iodixanol (Optiprep; Axis-Shield, Oslo, Norway) was added to a final concentration of 25% iodixanol. Four milliliters of this preparation was layered over a gradient of 4 ml of 30% and 4 ml of 35% iodixanol and then centrifuged at 10,000 × *g* for 20 min in a JA 20 rotor (Beckman). The pure nuclear band at the 30-to-35% interface was removed, and HHV-8 DNA was extracted by the use of DNeasy columns (Qiagen). The purity of the nuclear preparations was assessed by immunoblots using anti-lamin B antibodies, and cytoskeletal contamination was assessed by the use of anti-β-actin and anti-α-tubulin antibodies.

Western blot analysis. Total cell lysates (10 μg) were resolved in SDS-PAGE gels, transferred to nitrocellulose membranes, and immunoblotted with antibodies. Immunoreactive bands were then developed by enhanced chemiluminescence reactions (Perkin-Elmer) and quantified by standard protocols (50).

Affinity and coprecipitation assays. Affinity precipitation reactions using the GST–Rho-binding domain (RBD) of rhotekin (GST-RBD), which precipitated GTP-bound RhoA, and the GST–Rac-binding domain of PAK1 (PBD), which precipitated GTP-bound Rac or Cdc42, were done per the manufacturer's recommendations (Cytoskeleton Inc., Denver, Colo.) to determine the amounts of activated cellular RhoA, Rac1, and Cdc42 after HHV-8 infection. Briefly, cells were treated with agonists for different time periods, washed with phosphate-buffered saline (PBS), and lysed in RIPA buffer (50). The lysates were clarified, normalized to equal amounts of total proteins, and incubated with glutathione beads containing bound GST-PBD or GST-RBD for 90 min at 4°C. Bound Rac1 and RhoA were resolved by SDS–12% PAGE and immunoblotted with rabbit polyclonal antibodies against Rac1, Cdc42, and RhoA. For analyses of the association of Dia2 with RhoA, coaffinity precipitation was performed. Lysates were treated with GST-RBD beads to precipitate the activated GTP-bound RhoA. After being washed, the beads were boiled in 2× sample buffer, resolved by SDS–7.5% PAGE, and immunoblotted with rabbit anti-human Dia2 antibodies.

Cytotoxicity assay. The cytotoxicities of various inhibitors were assessed by use of a lactate dehydrogenase (LDH) cytotoxicity assay kit (Promega) as described previously (50).

Confocal microscopic analysis of HHV-8 trafficking in the cytoplasm. Serum-starved HFF cells in chamber slides were preincubated with nocodazole or LY294002 before being infected with HHV-8 at ~50 copies per cell. At 1 h p.i., the cells were washed, fixed for 15 min with 3.7% formaldehyde in PBS at room temperature, permeabilized for 3 min with 0.1% Triton X-100, and blocked for 30 min with 10% normal goat serum (Sigma) in PBS. The cells were incubated with a 1:100 dilution of rabbit polyclonal immunoglobulin G (IgG) against the HHV-8 capsid ORF65 protein (45) and with a 1:500 dilution of a mouse anti-α-tubulin MAb for 1 h at room temperature. After being washed with PBS, the cells were incubated with goat anti-rabbit IgG–Alexa 488 and goat anti-mouse–Alexa 594 (10 μg/ml) for 1 h at room temperature, washed, and mounted with a slowly fading antifade reagent containing DAPI (4′,6′-diamidino-2-phenylindole). The slides were examined with an LSM 510 confocal microscope and software version 2.8 (Carl Zeiss), and double staining was analyzed by use of the 495- and 590-nm bands of laser lines from a water-cooled argon-krypton laser. The digital images were processed with the LSM Image browser and Adobe Photoshop 5.5.

RESULTS

Depolymerization of microtubules, but not microfilaments, reduces infection by HHV-8. HHV-8 enters target cells within minutes after infection (3, 6, 43), which is accompanied by the formation of actin stress fibers, lamellipodia, and filopodia, an indication of Rho GTPase induction and modulation of the cytoskeleton during the early stages of infection (50). To investigate the role of HHV-8-induced cytoskeletal dynamics in the infectious process, we first analyzed the effect of depolymerization of the MTs by nocodazole and depolymerization of the actin MFs by cyto D and lat A (26) on GFP–HHV-8 infection. HFF cells that had been preincubated with nontoxic doses of nocodazole, cyto D, and lat A for 1 h at 37°C were infected with GFP–HHV-8 for 2 h in the presence of inhibitors. Under these conditions, immunostaining revealed the complete depolymerization of MTs (data not shown). The target cells were washed to remove the inhibitors and unbound virus and then further incubated for 3 days before enumerating GFP-expressing cells indicative of HHV-8 infection. Nocodazole inhibited GFP–HHV-8 infection significantly in a dose-dependent manner, with about 62% ± 3% and 73% ± 4% inhibition concentrations of 5 and 10 μg/ml, respectively (Fig. 1A). In contrast, cyto D and lat A did not alter the infection significantly even at concentrations of 10 μg/ml and 10 μM,

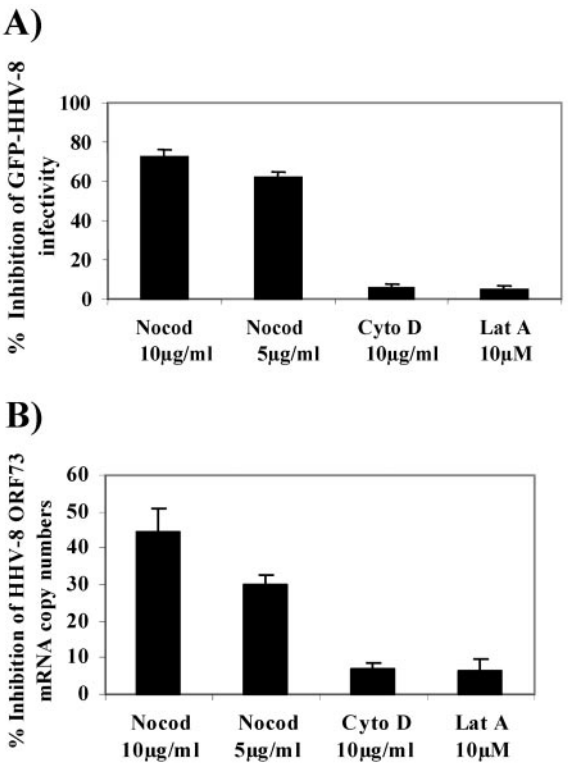

FIG. 1. Intact microtubules (MTs) are required for target cell infection by HHV-8. (A) MT depolymerization inhibits GFP–HHV-8 infectivity. HFF cell monolayers in eight-well chamber slides were incubated with Dulbecco's modified Eagle's medium (DMEM) containing different nontoxic concentrations of MT-depolymerizing nocodazole (Nocod) or MF-depolymerizing cyto D or lat A at 37°C for 1 h before being infected with GFP–HHV-8. The cells were incubated with virus for 2.5 h at 37°C in the presence of inhibitors, washed, and incubated with growth medium for 3 days at 37°C. Green fluorescent cells indicative of GFP–HHV-8 entry and infection were counted. In control wells, approximately 300 GFP-expressing cells were detected per well. Each reaction was done in triplicate, and each bar represents the mean ± standard deviation (SD) for three experiments. (B) Nocodazole inhibits HHV-8 ORF73 mRNA expression. HFF cells or HFF cells preincubated with nontoxic doses of nocodazole, cyto D, or lat A were infected with GFP–HHV-8 at a multiplicity of infection (MOI) of 5 DNA copies/cell for 2.5 h, washed, and incubated in fresh medium for 8 h. Total cellular RNAs were analyzed by real-time RT-PCRs using gene-specific Taqman probes to quantitate the HHV-8 ORF73 mRNA. Known concentrations of gene-specific transcripts from an ORF73 clone were used as standards. All samples were used in separate real-time PCRs without RT to confirm the absence of contaminating DNA. The relative copy numbers of the transcripts were calculated and normalized to GAPDH control reaction values. Data are presented as percentages of the inhibition of ORF73 mRNA copy numbers obtained when the cells were incubated with virus alone. Each reaction was done in duplicate, and each point represents the mean ± SD for three experiments.

respectively (Fig. 1A), and these treatments were shown previously to profoundly alter actin polymerization (29).

To further ascertain the specificity of GFP–HHV-8 inhibition by nocodazole, we quantified the relative copy numbers of HHV-8 latency-associated ORF73 mRNA by real-time RT-PCR (43) and normalized these numbers to the numbers of glyceraldehyde-3-phosphate (GAPDH) copies in the same samples. Preincubation of the virus with 100 μg of heparin/ml blocked >80% of HHV-8 ORF73 gene expression (data not shown). Nocodazole reduced the ORF73 expression significantly, with about 30% ± 3% and 45% ± 7% inhibition at concentrations of 5 and 10 μg/ml, respectively (Fig. 1B). The expression levels of cellular GAPDH gene expression were unaffected. In contrast, cyto D and lat A did not affect ORF73 expression (Fig. 1B). These results suggested that HHV-8 requires intact microtubules for efficient infection of target cells.

HHV-8 infection modulates host cell microtubule dynamics. To determine whether HHV-8 infection affects target cell MT dynamics, we next investigated the polymerization (aggregation) of MTs at early times p.i. Serum-starved HFF cells were infected with HHV-8 (five copies per cell) for various times, fixed, permeabilized, and stained for MTs by the use of anti-tubulin antibodies. Serum-starved uninfected cells exhibited the classical pattern of finely-spread-out loose bundles of MTs radiating from the perinuclear nucleation center of MTs, the microtubular organizing center (MTOC), towards the edges of the cell (Fig. 2A, panel 1). As early as 30 min p.i., HHV-8 induced the aggregation of MTs, leading to an increased thickening of MT bundles (Fig. 2A, panel 2). These HHV-8-induced changes were comparable to the effects observed in HFF cells 30 min after a treatment with 20 ng of LPA/ml (data not shown). The HHV-8-induced thickening of MTs into bundles and the aggregation of MTs were sustained for at least 90 min p.i. (Fig. 2A, panels 3 and 4). By about 2 h p.i., the MTs returned to the classical spread-out pattern (Fig. 2A, panels 5 and 6). These data demonstrate a transient reorganization of the MT network into bundles, replacing the normal MT cytoskeletal morphology, and suggest that there is a modulation of microtubule dynamics early during infection by HHV-8.

HHV-8 infection modulates MTs and induces hyperacetylation. Under physiological conditions, acetylation and deacetylation act as powerful and dynamic means of controlling MT dynamics (55). Cellular structures that cross-link MTs along their length or cap their ends are known to cause acetylation on MTs and their stabilization (55). Since hyperacetylation is a quantitative indication of changes in MT stabilization, to confirm the influence of HHV-8 on MT dynamics, we next quantified the levels of MT acetylation by Western blot analysis. Uninfected cells contained a moderate level of acetylated MTs (Fig. 2B, lane 1). In contrast, MTs were heavily acetylated in the infected cells, with >2.5-, 4-, and 3-fold increases in acetylation by 30 min, 1 h, and 2 h p.i., respectively (Fig. 2B, lanes 2 to 4, and Fig. 2C), which returned to the basal level by 3 h p.i. (Fig. 2B, lane 5). The levels of total α-tubulin remained unaltered, thus demonstrating the specificity of acetylation (Fig. 2B). The HHV-8-induced hyperacetylation was comparable to the induction by LPA, a known inducer (Fig. 2B, lanes 6 to 8). The observed acetylation was also confirmed by determining the relative amounts of acetylated tubulin in HHV-8-infected cells by an immunofluorescence assay (data not shown). MT hyperacetylation further suggested that HHV-8 profoundly influences the MT dynamics during the early stages of target cell infection.

Microtubule depolymerizing agents reduce the transport of HHV-8 DNA to the nucleus. Our earlier studies have shown that HHV-8 internalization via endocytic vesicles in HFF and BJAB cells occurs as early as 5 min p.i. (3, 6). We also detected internalized viral DNA in target cells as early as 5 min p.i. whose levels increased rapidly during the first 60 to 90 min of infection, reaching a plateau around 90 to 120 min p.i. (43). Since the reduction in HHV-8 infectivity and ORF73 gene expression in cells with depolymerized MTs (Fig. 1A and B) may have been due to interference in virus binding or internalization or at postentry steps such as transport of the virus capsid to the cell nucleus and delivery of viral DNA to the nucleus, we next investigated the stage at which MTs play a role in HHV-8 infection. As an initial step, we examined the kinetics of HHV-8 DNA delivery into infected cell nuclei. HFF cells were infected with HHV-8 for various times, and pure nuclear fractions were isolated by cell lysis and gradient purification (Fig. 3A). Nuclear fractions were positive for the nuclear marker lamin B (Fig. 3A, top panel, lane 2). In contrast, the cytoskeletal marker detected by anti-α-tubulin antibodies (Fig. 3A, bottom panel, lane 2) or anti-β-actin antibodies (data not shown) did not show any reactivity with the nuclear fractions. The saturation of enhanced chemiluminescence (ECL) reactions by a maximum exposure for 20 min also failed to detect a positive reaction with α-tubulin or β-actin antibodies (data not shown). These results demonstrated the absence of cytoskeletal contamination in our purified nuclear fractions. DNAs were extracted from the isolated nuclei, and 100 ng of total DNA was quantified by real-time DNA PCR with HHV-8 ORF73 primers. Relatively rapid nuclear delivery of HHV-8 DNA, detectable as early as 30 min p.i., was observed, and the DNA copies continued to accumulate over time, reaching a plateau between 180 and 240 min p.i. (Fig. 3B).

HHV-8 interacts with cell surface HS during the initial attachment stage of infection (3). We next determined whether the inhibition of HHV-8 infection in cells with depolymerized MTs was due to the inhibitors' ability to block virus binding to the target cells. Similar to our previous findings (3), heparin at a concentration of 10 μg/ml inhibited >90% of [^{3}H]thymidine-labeled HHV-8 binding to HFF cells (Fig. 3C, open bars). In contrast, no effect was seen with nocodazole, Colcemid, cyto D, paclitaxel, and NH_4Cl (Fig. 3C, open bars). To determine whether the reduction in HHV-8 infectivity and ORF73 gene expression in cells with depolymerized MTs was due to interference at the virus internalization stage of infection, we preincubated cells with various drugs that disrupt MFs or MTs for 1 h, infected them with the virus for 2 h, washed them to remove unbound virus, and treated them with trypsin-EDTA to remove bound but noninternalized virus. The total DNAs were isolated, and relative copy numbers of HHV-8 ORF73 were estimated by real-time DNA PCR. HHV-8 internalization was inhibited ~90% by heparin, and no effect was seen with nocodazole, Colcemid, cyto D, paclitaxel, and NH_4Cl (Fig. 3C, closed bars). These results demonstrated that nocodazole and Colcemid inhibit at postattachment and postinternalization stages of infection.

To determine whether the reduction in HHV-8 infectivity

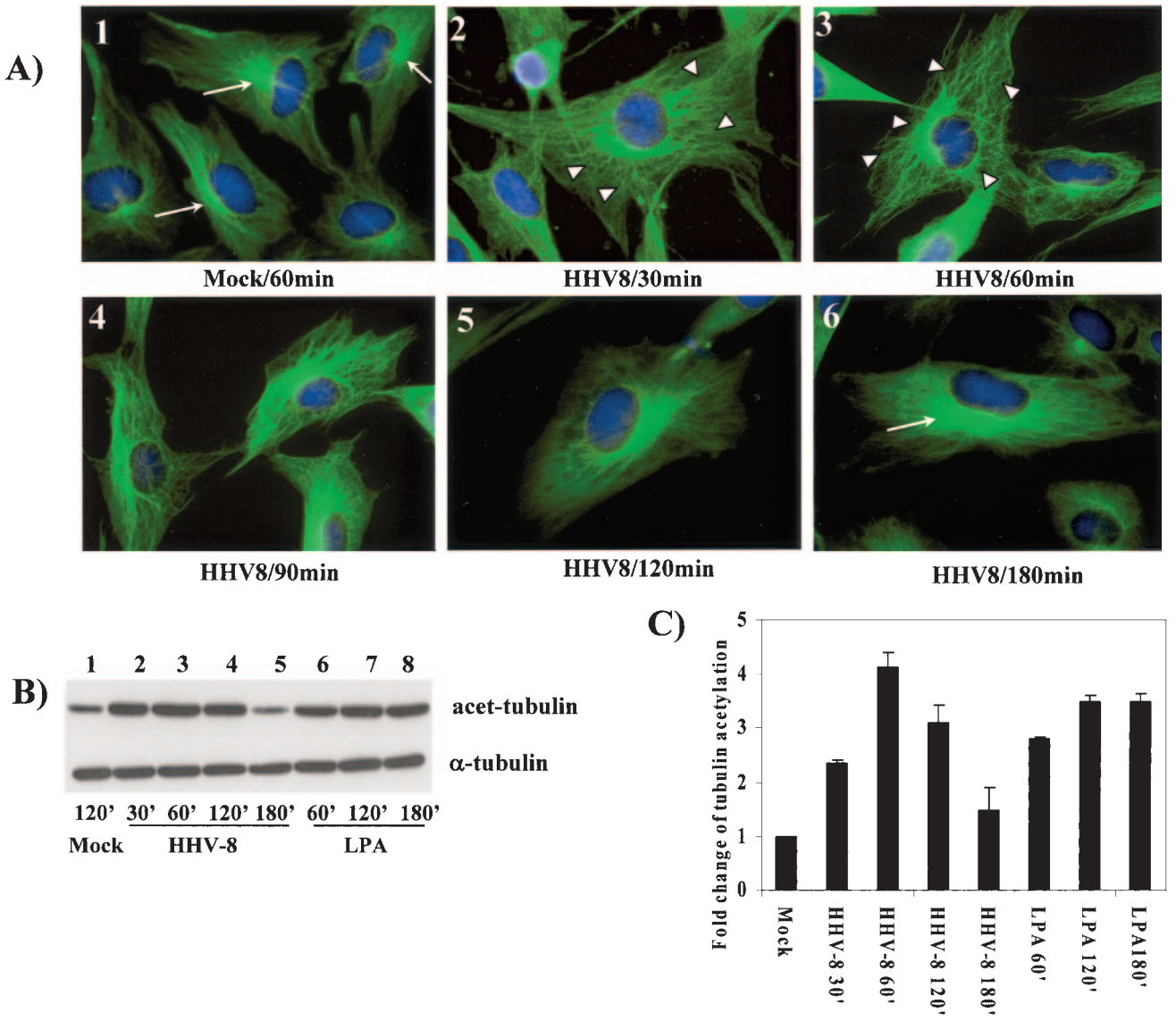

FIG. 2. (A) HHV-8 interaction with target cells induces MT polymerization. Serum-starved HFF cells were either mock treated with DMEM (panel 1) or infected with 5 DNA copies of GFP–HHV-8/cell (panels 2 to 6). At different time points, the cells were washed, fixed in 4% formaldehyde, washed, and permeabilized in 0.1% Triton X-100 at room temperature. The cells were incubated for 30 min with 1% bovine serum albumin and then with a mouse anti-α-tubulin MAb (diluted 1:500 in 1% bovine serum albumin) at room temperature for 45 min. These cells were washed, incubated with anti-mouse IgG–fluorescein isothiocyanate for 30 min, washed, mounted in a slowly fading reagent containing DAPI, and visualized under a fluorescence microscope. Narrow arrows indicate the microtubular organizing centers (MTOC), and arrowheads indicate MT bundling. Magnification,×60. (B) HHV-8-induced MT dynamics involve the hyperacetylation of tubulin. Serum-starved HFF cells were either mock infected or infected with 5 DNA copies of HHV-8/cell for the indicated times and then were lysed with RIPA lysis buffer. Ten micrograms of lysate was resolved by SDS–10% PAGE and immunoblotted with a MAb against acetylated tubulin (top) or total α-tubulin (bottom). Immunoreactive bands were developed by standard ECL reactions. (C) The band intensities in panel B were quantitated, and the acetylated tubulin in mock-infected HFF cells was considered a onefold induction for comparisons to infected cells. Each bar represents the mean ± SD for three experiments.

and ORF73 gene expression by nocodazole and Colcemid was due to interference at postentry steps such as transport of the virus capsid to the cell nucleus and delivery of the viral DNA to the nucleus, we preincubated HFF cells with the MT-specific inhibitors nocodazole and Colcemid and the MF-specific inhibitors cyto D and lat A for 1 h at 37°C. These cells were infected with HHV-8 at 37°C in the presence of inhibitor for 3 h, and infected cell nucleus-associated HHV-8 DNA copy numbers were quantified. Our earlier studies demonstrated a significant reduction in GFP–HHV-8 infectivity and ORF73 mRNA expression when HFF cells were pretreated with NH_4Cl, a lysosomotrophic agent that inhibits the acidification of endosomal compartments (6). HHV-8 nuclear trafficking was also reduced about 68% ± 3% with a 100 mM concentration of NH_4Cl (Fig. 3D). Nocodazole and Colcemid incubation significantly blocked viral DNA delivery to the nucleus in a dose-dependent manner (Fig. 3D). In contrast, pretreatment with cyto D did not inhibit the nuclear delivery of HHV-8

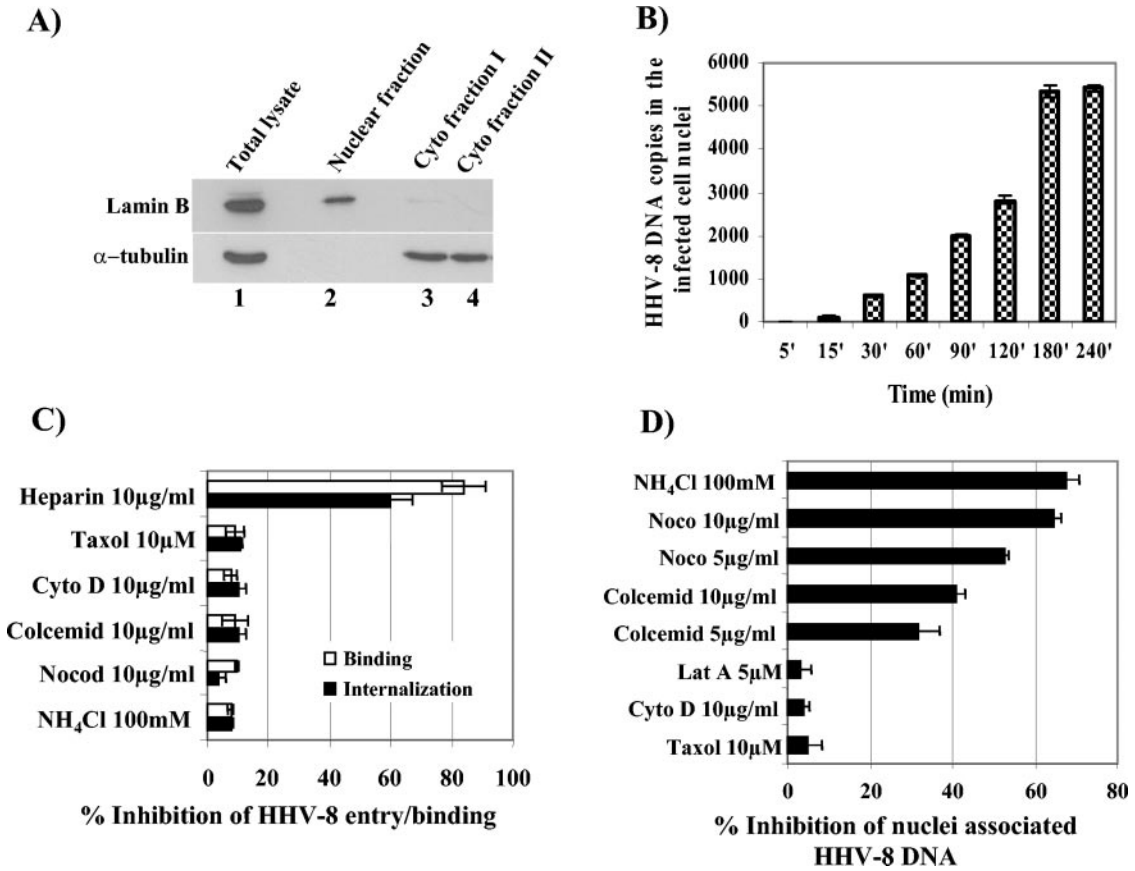

FIG. 3. HHV-8-induced MT dynamics influence the nuclear delivery of HHV-8 DNA. (A) Purification of infected cell nuclei. Uninfected and HHV-8-infected HFF cells were washed with PBS, treated with trypsin-EDTA to remove noninternalized virus, washed, suspended in lysis buffer, and allowed to swell on ice for 5 min. Nuclei were pelleted at 500 × *g* for 5 min, and the supernatant was collected as cytoplasmic fraction I. The nuclear pellet was resuspended in lysis buffer, and the extraction was repeated once to obtain cytoplasmic fraction II. The remaining nuclear pellet was resuspended in nuclear homogenization buffer and iodixanol (Optiprep), layered over a gradient of 30 and 35% Optiprep, and centrifuged at 10,000 × *g* for 20 min. The nuclear fraction at the 30 to 35% Optiprep interface was collected. Immunoblot reactions were performed to detect the total cell lysate (lane 1), cytoplasmic fractions I and II (lanes 3 and 4), and the purified nuclear fraction (lane 2) by the use of monoclonal antibodies against lamin B and α-tubulin. (B) Kinetics of HHV-8 DNA delivery into infected cell nuclei. Nuclear fractions from HFF cells infected at 5 DNA copies/cell for the desired time points were isolated, and the total DNA was isolated, normalized to contain 100 ng/5 μl, and analyzed by real-time DNA PCR with HHV-8 ORF73 primers. Copy standards and nontemplate controls were run in parallel. The relative viral DNA copy numbers were calculated from a standard graph generated by real-time PCRs of known concentrations of a cloned ORF73 gene. Each reaction was done in duplicate, and each bar represents the mean ± SD for three experiments. (C) MT-depolymerizing agents do not affect HHV-8 binding and internalization. HFF cells were either left untreated or preincubated with various drugs that disrupt MFs or MTs for 1 h before being incubated with [^{3}H]thymidine-labeled, purified HHV-8 virus for binding assays (5,000 cpm) or with unlabeled HHV-8 for internalization assays. As a control, the virus was preincubated with 10 μg of heparin/ml for 1 h at 37°C before being added to the cells. After incubation for 90 min at 4°C with the labeled virus, the cells were washed, lysed, precipitated with trichloroacetic acid, and counted. The cell-associated virus count per minute in the presence of each different treatment was calculated as the percentage of inhibition of virus binding. Each reaction was done in triplicate, and each bar represents the average ± SD for three experiments (open bars). For the internalization assay, after 2 h of incubation with unlabeled virus, the cells were washed twice with PBS to remove the unbound virus, treated with trypsin-EDTA for 5 min at 37°C to remove the bound but noninternalized virus, and washed, and total DNAs were isolated and HHV-8 ORF73 copies were estimated by real-time DNA PCR. The C_t values were used to plot a standard graph and to calculate the relative copy numbers of viral DNA in the samples. Data are presented as percentages of the inhibition of HHV-8 DNA internalization obtained when the cells were incubated with virus alone. Each reaction was done in duplicate, and each bar represents the average ± SD for three experiments (black bars). (D) Depolymerization of MTs reduces nuclear delivery of HHV-8 DNA. HFF cells or HFF cells preincubated for 1 h with nontoxic doses of NH_4Cl, nocodazole, Colcemid, paclitaxel, cyto D, and lat A were infected with 5 DNA copies of HHV-8/cell for 3 h in the presence of inhibitors. The purification of nuclear fractions and real-time DNA PCRs estimating the numbers of HHV-8 ORF73 copies were done as described above for panels A to C. Data are presented as percentages of inhibition of HHV-8 DNA associated with cell nuclei relative to that of cells incubated with virus alone. Each reaction was done in duplicate, and each bar represents the mean ± SD for three experiments.

DNA (Fig. 3D). To confirm that the lack of effect by cyto D was not due to the slow kinetics of MF depolymerization, we also treated HFF cells with 5 μM lat A, which is known to have much more rapid kinetics of MF depolymerization than cyto D. The lat A inhibitor also did not significantly affect the nuclear trafficking of HHV-8 DNA (Fig. 3D). The treatment of cells with paclitaxel (Taxol), the prototypic microtubule-stabilizing drug affecting the tubulin-microtubule equilibrium, did not affect nuclear transport (Fig. 3D), thus indicating a requirement for the dynamic nature of the MTs in HHV-8 DNA

transport. These studies suggested that the inhibition of HHV-8 infectivity by nocodazole may be due to interference in the transport of the virus capsid and the delivery of viral DNA into the nuclei and that HHV-8-induced MT dynamics play a vital role in the nuclear trafficking of viral DNA. These results also suggested that although HHV-8 induced actin MF remodeling (50), the MFs may not play a significant role in the infectious process, at least during the early phases of infection.

HHV-8 induces activation of RhoA and Rac1 GTPases in target cells. Even though many viruses are known to exploit the MTs and their associated motors for nuclear trafficking (7, 24, 28, 38, 44, 47, 61, 62, 69), the host signaling pathways exploited by these viruses to mediate this process and the mechanism of signal induction remain largely unknown. Recent studies have demonstrated potential links between RhoA, Rac1, and Cdc42 GTPases and microtubule dynamics (12, 22, 37, 40, 53, 68). Since our studies have demonstrated the integrin-dependent activation of PI-3K and Rho GTPase as well as cytoskeletal rearrangements in HHV-8-infected cells (50), we next examined the potential links between HHV-8-induced signaling pathways and the regulation of MT dynamics.

As a first step, we examined Rho, Rac, and Cdc42 activation during HHV-8 infection by affinity precipitation using GST-RBD or GST-PBD followed by Western blot analysis. Compared to the case for uninfected cells, the RhoA-GTP and Rac1-GTP levels in infected cells were increased about 3.0- to 5.0-fold (Fig. 4), and no induction of Cdc42 was observed (data not shown). Although peak levels of RhoA and Rac1 activation were observed at 5 min p.i., the Rac1-GTP activation was more sustained than the RhoA-GTP induction (Fig. 4). HHV-8 induced robust RhoA- and Rac1-GTP activities in infected cells which were comparable to induction by LPA (Fig. 4A, lanes 7 and 8) or phorbol myristate acetate (PMA) (Fig. 4B, lanes 6 to 8). The total RhoA or Rac level in infected cells was unchanged (Fig. 4A and B, bottom panels), thus demonstrating the specificity of GTP activation. These results further supported our earlier morphological observation that Rho GTPases are activated by HHV-8 early during infection (50). HHV-8 interacts with the α3β1 integrin via its gB protein, and virus binding studies suggested that α3β1 integrin is one of HHV-8's entry receptors (5, 60). In order to test the specificity of HHV-8-induced Rho GTPase activation, we preincubated HHV-8 with different concentrations of soluble α3β1 or control α5β1 integrin before adding the virus to target cells for 5 min. As observed before (Fig. 4), HHV-8 induced robust RhoA- and Rac1-GTP activities in infected cells (Fig. 5A and B, lanes 2). A dose-dependent reduction in the HHV-8-induced RhoA- and Rac1-GTP activities was observed when the virus was preincubated with α3β1 integrin (Fig. 5A and B, lanes 3 and 4, and Fig. 5C). No effect was seen with the α5β1 integrin treatment (Fig. 5A and B, lanes 5, and Fig. 5C). Minimal Rho GTPase activation by HHV-8 was observed in cells that were preincubated with CdTxB, a specific inhibitor of Rho GTPases (Fig. 5A and B, lanes 6).

Modulation of Rho GTPases affects nuclear delivery of HHV-8 DNA. The glucosyltransferase CdTxB targets different Rho GTPases and efficiently blocks the interaction of Rho GTPases with their effectors, thus resulting in functionally inactive GTPases (1, 18). In contrast, *E. coli* cytotoxic necrotizing factor 1 (CNF-1) activates Rho GTPases through the deamidation of a pivotal glutamine residue (Glu 63 of Rho and Glu 61 of Cdc42 and Rac) involved in GTP hydrolysis (2). Upon deamidation, the intrinsic GAP-stimulated GTPase activity is blocked, thereby rendering the GTPase permanently active (2). These toxins are very specific for Rho GTPases and have been used extensively to study the roles of Rho GTPases in target cell infections by different pathogens (2, 40). When used at <300 ng/ml, CdTxB was nontoxic and induced 100% cell rounding without LDH release, whereas CNF-1 did not induce

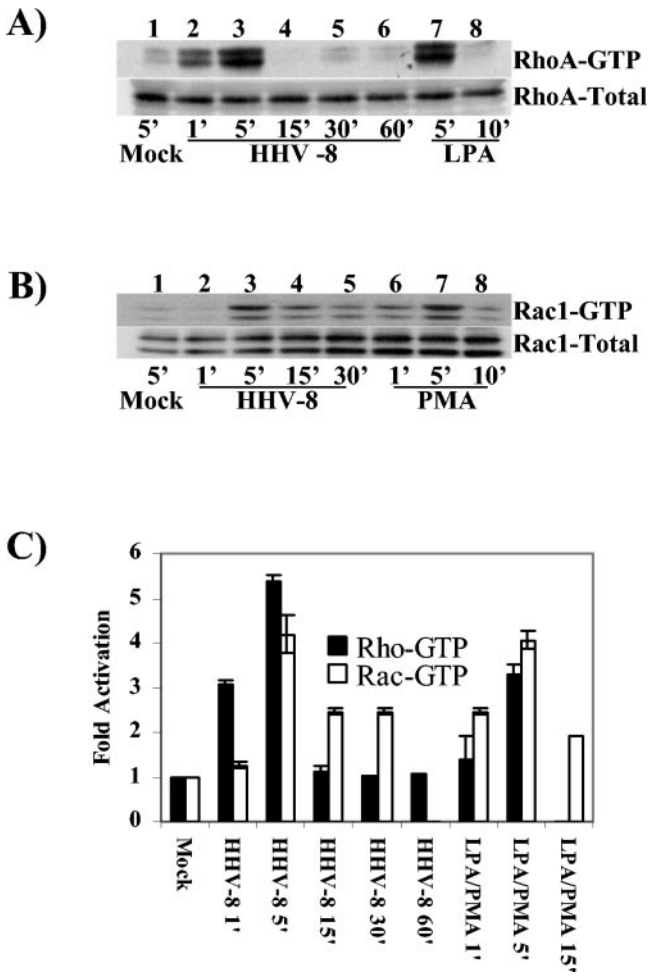

FIG. 4. HHV-8 induces RhoA and Rac1 GTPases in target cells. (A and B) Kinetics of RhoA and Rac1 induction. Equal amounts of HFF cell lysates from mock-infected cells (5 min), cells infected with HHV-8 at 5 DNA copies/cell (1, 5, 15, 30, or 60 min), or cells treated with 20 ng of LPA/ml or 100 ng of PMA/ml (5 and 10 min) were used to capture the GTP-bound forms of Rho GTPases by affinity precipitation with GST-RBD or GST-PBD beads. The proteins captured by beads were analyzed by SDS–12% PAGE and immunoblotted with anti-RhoA or anti-Rac1 antibodies (top panels of A and B, respectively). The bottom panels of A and B show normalized cell lysates analyzed for total RhoA or Rac1 as a loading control. (C) Quantitation of HHV-8-induced RhoA and Rac1 GTPases. The bands from panels A and B were scanned, and their intensities assessed and quantified, with GTP-bound RhoA (black bars) and Rac1 (open bars) in mock-infected cells being considered onefold activation for comparisons to infected cells. Each point represents the mean ± SD for three experiments. Note that there are no data for Rac1 at 60 min with virus and for RhoA at 15 min with PMA, as these experiments were not done.

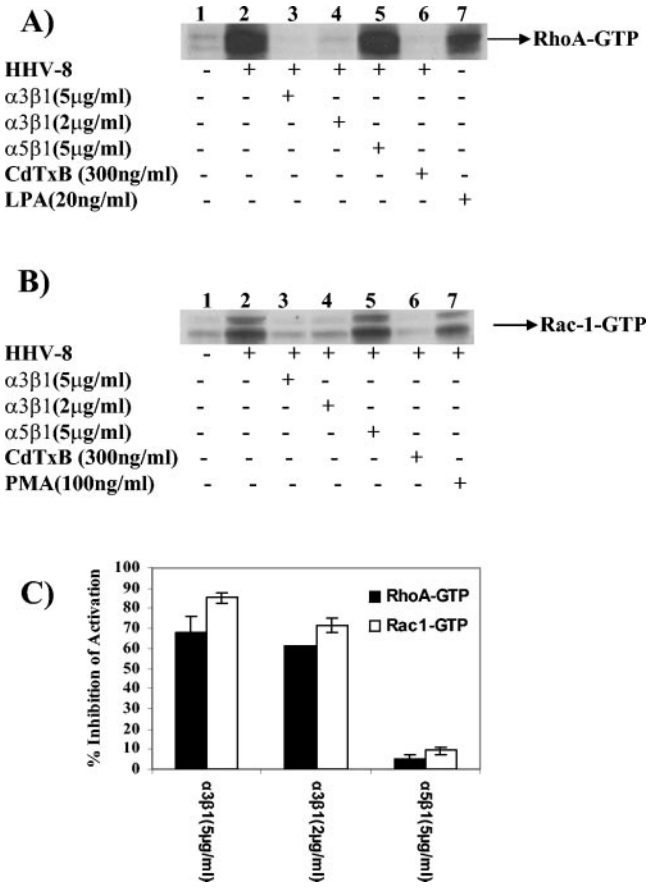

FIG. 5. Specificity of HHV-8-induced RhoA and Rac1 Rho GTPases. (A and B) Serum-starved HFF cells were either mock infected (lanes 1) or infected with HHV-8 at an MOI of 5 DNA copies/cell (lanes 2) for 5 min. In parallel experiments, HHV-8 was incubated with the indicated concentrations of soluble α3β1 or α5β1 integrin for 90 min at 37°C before infecting the cells for 5 min (lanes 2 to 4). The cells were also preincubated with CdTxB to inhibit Rho GTPases for 90 min before being infected with the virus for 5 min in the presence of toxin B (lanes 6). For controls, cells were induced with LPA or PMA for 5 min (lanes 7). Equal amounts of cell lysates were analyzed for the induction of RhoA and Rac1 GTPases per the procedures described in the legend for Fig. 4A and B. (C) The bands in panels A and B were scanned, and their intensities were assessed and quantified. Data are presented as percentages of the inhibition of GTP-bound RhoA (black bars) and Rac1 (open bars) obtained when the cells were incubated with virus alone. Each bar represents the mean ± SD for three experiments.

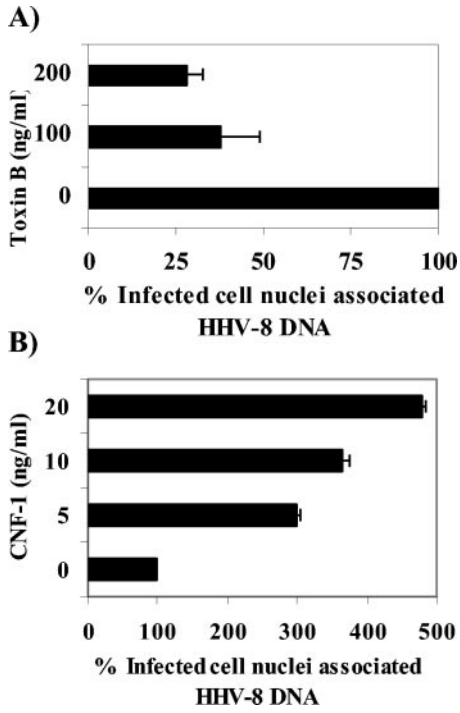

FIG. 6. Modulation of Rho GTPase influences nuclear delivery of HHV-8 DNA. HFF cells or HFF cells incubated with different concentrations of CdTxB for 90 min at 37°C (A) or CNF-1 for 4 h at 37°C (B) were infected with HHV-8 at 5 DNA copies/cell for 3 h. The cells were washed to remove the unbound virus, treated with trypsin-EDTA to remove the bound but noninternalized virus, and analyzed by real-time DNA PCR to estimate the HHV-8 DNA copy numbers associated with the infected cell nuclei (A and B) per the methods described in the legend to Fig. 3. Data are presented as percentages of HHV-8 DNA associated with infected cell nuclei (A and B) relative to that in cells that were incubated with virus alone. Each reaction was done in duplicate, and each bar represents the mean ± SD for three experiments.

LDH release even when it was used at 10 μg/ml (data not shown).

For an investigation of whether RhoA or Rac1 activation is required for the nuclear transport of HHV-8, HFF cells that had been preincubated with nontoxic doses of CdTxB or CNF-1 were infected for 3 h, and the viral DNA was quantified by real-time DNA PCR. Dose-dependent decreases in the HHV-8 DNA copy numbers associated with infected cell nuclei were observed for the CdTxB pretreatment, with about 72 and 62% inhibition at concentrations of 200 and 100 ng/ml, respectively (Fig. 6A). In contrast, CNF-1 increased the nuclear trafficking of HHV-8 DNA substantially in a dose-dependent manner (Fig. 6B), with as much as a 500% increase at 20 ng/ml. These results suggest that there is an active involvement of HHV-8-induced Rho GTPases in the nuclear trafficking of viral DNA during the initial stages of infection.

HHV-8-induced Rho GTPases stabilize MTs by hyperacetylation. Our results suggest that HHV-8 entry activates Rho GTPases, the known modulators of MF and MT dynamics (13, 20, 52). In contrast to the MF depolymerizing agents, MT depolymerizing agents substantially inhibited viral trafficking in the cytoplasm and the delivery of viral DNA to the nucleus. To decipher the role of Rho GTPases in cytoskeletal dynamics, especially those of MTs during HHV-8 infection, we preincubated cells with CdTxB before incubating them with HHV-8 for 60 min. The cell lysates were tested for hyperacetylated MTs by Western blot analysis. Compared to the case for mock-treated HFF cells (Fig. 7A, lane 1), HHV-8 induced a significant level of α-tubulin hyperacetylation (Fig. 7A, lane 2). The treatment with CdTxB reduced the tubulin hyperacetylation in a dose-dependent manner (Fig. 7A, lanes 3 to 5, and Fig. 7B), with about 49, 71, and 78% reductions in acetylation at concentrations of 100, 200, and 300 ng/ml, respectively (Fig. 7B). These results suggested that HHV-8-induced Rho GTPases contribute to MT hyperacetylation and stabilization.

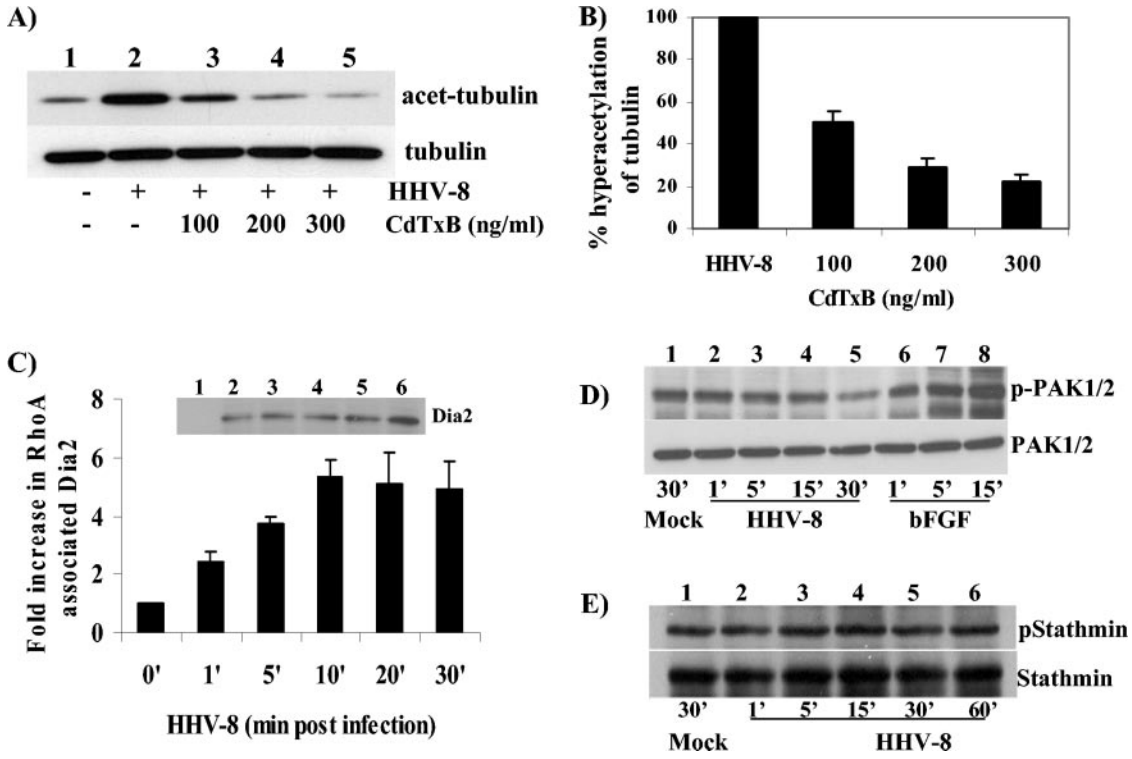

FIG. 7. Rho-GTPases regulate HHV-8-induced MT polymerization through RhoA and diaphanous 2. (A) Inhibition of Rho GTPase blocks MT hyperacetylation. HFF cells incubated with different concentrations of CdTxB were infected with HHV-8 at 5 DNA copies/cell for 60 min. Ten micrograms of lysate was resolved by SDS–10% PAGE and immunoblotted with a MAb against acetylated tubulin (top) or total α-tubulin (bottom). Immunoreactive bands were developed by standard ECL reactions. (B) The band intensities in panel A were quantitated, with the acetylated tubulin in mock-infected HFF cells being considered onefold activation for comparisons to infected cells. Data are presented as percentages of the inhibition of tubulin hyperacetylation when the cells were incubated with virus alone. Each bar represents the mean ± SD for three experiments. (C) GTP-bound RhoA associates with diaphanous 2 upon HHV-8 infection. Serum-starved uninfected HFF cells (lane 1) or cells infected with HHV-8 at an MOI of 5 DNA copies/cell for 1, 5, 10, 20, and 30 min (lanes 2 to 6) were lysed with RIPA buffer, and activated GTP-bound RhoA was affinity precipitated with GST-RBD beads. The beads were washed, boiled in 2× sample buffer, resolved by SDS–7.5% PAGE, and immunoblotted with an antibody detecting total Dia2. Immunoreactive bands were developed by ECL reactions, and band intensities were scanned and quantified. Dia2 associated with RhoA in mock-infected HFF cells was considered onefold activation for comparisons to infected cells. Each bar represents the mean ± SD for three experiments. (D and E) PAK and stathmin are not phosphorylated by HHV-8 infection. Serum-starved uninfected HFF cells, cells infected with HHV-8 for different time periods, or cells stimulated with basic fibroblast growth factor were lysed with RIPA buffer, and equal amounts of protein were resolved by SDS–10% PAGE and immunoblotted with an antibody detecting phosphorylated PAK1/2 or total PAK (D, upper and lower panels, respectively) or phosphorylated stathmin or total stathmin (E, upper and lower panels, respectively).

HHV-8-induced RhoA GTPase activates diaphanous 2, which is involved in MT dynamic modulation. Since the studies described above demonstrated the importance of HHV-8-induced Rho GTPases in the nuclear trafficking of viral DNA and the regulation of MT dynamics, we next examined the contributing signaling pathways. Even though the Rho GTPases are believed to be essential for the regulation of MT dynamics, only recently have studies suggested that these may be mediated by the activation of several accessory molecules (27, 33, 37, 53). There is growing evidence that RhoA activates the diaphanous-related formin family molecules Dia1 and Dia2 (37, 53). Formins are one of the four major classes of poly-L-proline-containing proteins that form part of the signal transduction cascade that leads to rearrangement of the cytoskeleton. Rac and Cdc42 activate PAK1/2 (p21-activated kinase), which in turn inactivates the MT destabilizer Op18 (stathmin), thus promoting polymer growth (27). Rac and Cdc42 have also been shown to interact with MTs through a common effector, IQ-GAP, which binds CLIP-170, an MT-associated protein that is recruited to the plus ends of polymerizing MTs (33).

To determine whether HHV-8-induced RhoA activates Dia2, we examined the coprecipitation of Dia2 with activated RhoA-GTP. Activated RhoA-GTP that was affinity precipitated with GST-RBD beads was immunoblotted with antibodies against Dia2, and phosphorylation-specific antibodies were used to demonstrate the Rac- and Cdc42-dependent phosphorylation of PAK1/2 and stathmin. HHV-8 infection increased the RhoA-dependent activation of Dia2 in a time-dependent manner (Fig. 7C). The activation of Dia2 was seen as early as 1 min p.i., continued to increase for the initial 10 min, reaching a plateau between 20 and 30 min (Fig. 7C), and was sustained for about 60 min before reaching the baseline (data not shown). In contrast, no significant phosphorylation of Rac- and Cdc42-dependent PAK1/2 was observed in infected cells (Fig. 7D). The phosphorylation of Rac- and Cdc42-dependent stath-

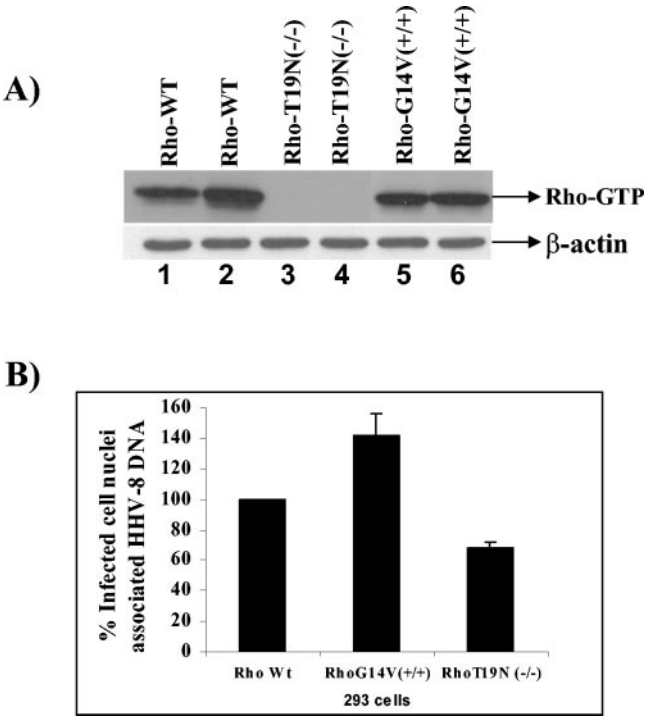

FIG. 8. (A) Characterization of Rho mutants. 293 cell lines transfected with plasmids expressing different forms of RhoA (wild type, $G14V^{+/+}$, or $T19N^{-/-}$) were established and characterized by a GTP-loading assay (top panel). As loading controls, lysates were resolved in parallel and Western blotted with β-actin antibodies (bottom panel). Lanes were loaded with duplicate samples. (B) Effect of Rho mutants on HHV-8 nuclear delivery. 293 cell lines expressing Rho mutants were infected with HHV-8 at 5 DNA copies/cell for 3 h. The cells were washed to remove the unbound virus and treated with trypsin-EDTA to remove the bound but noninternalized virus. Pure nuclear fractions were isolated and analyzed by real-time DNA PCR to estimate the HHV-8 DNA copy numbers associated with the infected cell nuclei per the methods described in the legend to Fig. 3. Data are presented as percentages of HHV-8 DNA associated with the infected cell nuclei. Each reaction was done in duplicate, and each point represents the mean ± SD for three experiments.

min was also not observed in infected cells (Fig. 7E). The activation of Dia2 by RhoA has been shown to stimulate the formation of stable microtubules that are capped, and Dia promotes this capping by directly binding to microtubules (53). Together, these results suggest that HHV-8-induced Rho GTPases probably control MT dynamics via the RhoA-GTP-dependent activation of diaphanous 2 and thus facilitate efficient trafficking of viral DNA to infected cell nuclei.

To ascertain the specificity of RhoA GTPase effects during HHV-8 infection, we established 293 cell lines expressing various forms of RhoA mutants, characterized the cells, and infected them with HHV-8 (Fig. 8A). An examination of infected cell nucleus-associated HHV-8 DNA demonstrated a 40 to 50% increase in cells transfected with a constitutively active RhoA mutant compared to wild-type cells (Fig. 8B). In contrast, 293 cells expressing dominant-negative RhoA demonstrated a 32 to 35% reduction in nucleus-associated viral DNA copies. These results clearly demonstrate the role of RhoA GTPase in the nuclear trafficking of HHV-8.

HHV-8 capsids colocalize with microtubules, and MT depolymerizing nocodazole and a PI-3K inhibitor reduce cytoplasmic trafficking of HHV-8. The significant reduction in the nuclear accumulation of HHV-8 DNA by MT depolymerization and the modulation of MT dynamics by HHV-8-induced RhoA GTPase clearly demonstrated the important role of the MT network in HHV-8 trafficking in the infected cell. To confirm the above biochemical observations morphologically, we examined the infected cells by confocal microscopy. Untreated cells or cells that were preincubated with 10 μg of the MT inhibitor nocodazole/ml or a 50 μM concentration of the PI-3K inhibitor LY294002 were infected with HHV-8 at ~50 copies/cell and examined after 1 h, a time point when a significant amount of nuclear accumulation of HHV-8 DNA was beginning to occur (Fig. 3B). To visualize the incoming viral capsids, we used well-characterized rabbit antibodies against the HHV-8 capsid protein ORF65 (45). Anti-tubulin antibodies were used to visualize the MT cytoskeleton.

The confocal microscopic images were obtained sequentially with 1-μm-thick sections, and the representative sections shown in Fig. 9 are through the middle of the cell. In the absence of drug treatments, the ORF65 antibody reactivity demonstrated the accumulation of HHV-8 capsids in the cytoplasm and near the vicinity of infected cell nuclei. Some examples are shown in Fig. 9D to F. Similar results were obtained when the incubation was extended to 3 h, and these morphological observations correlated well with the results of the nuclear delivery assay (Fig. 3B). When the anti-ORF65 reactivity was merged with MT staining, viral capsids were observed as fine dots connected to the microtubules, and the majority of the capsids near the proximity of nuclei appeared to be colocalized with the MTs (Fig. 9D to F). The specificity of these observations was shown by the absence of staining with preimmune IgG antibodies (Fig. 9A to C). Disruption of the MT network by nocodazole significantly distributed the MT network (Fig. 9G to I). In these cells, the ORF65 antibody reactivity was observed only in the periphery and was barely detectable in the cytoplasm, and the perinuclear accumulation of viral capsids was significantly decreased (Fig. 9G to I). The effect of nocodazole was reversible since when the infected cells were analyzed 1 h after drug removal, the MTs had repolymerized, accompanied by the reappearance of viral capsids near the nuclear rim (data not shown).

PI-3K induction has been observed as an upstream event of Rho GTPase activation in the HHV-8- or HHV-8 gB-induced signaling pathways (50, 60). The inhibition of PI-3K by LY294002 blocked the HHV-8-induced Rho GTPases and the accompanying morphological changes and blocked the entry of the virus into the target cells (50, 60). The treatment with LY294002 also resulted in disruption of the MT network and, consequently, the absence of perinuclear accumulation of the HHV-8 capsids (Fig. 9J to L). The ability of PI-3K inhibitors to block >80% of HHV-8 entry into target cells (60), together with the involvement of PI-3K in Rho GTPase activation involved in the formation of endocytic vesicles, their fission, the movement of vesicles in the cytoplasm, and the modulation of microtubule dynamics, suggests that the observed weak capsid signal in PI-3K inhibitor-treated cells was probably not due to the nonspecific effect of the drugs but to a specific effect on PI-3K and the associated signaling pathways preventing effi-

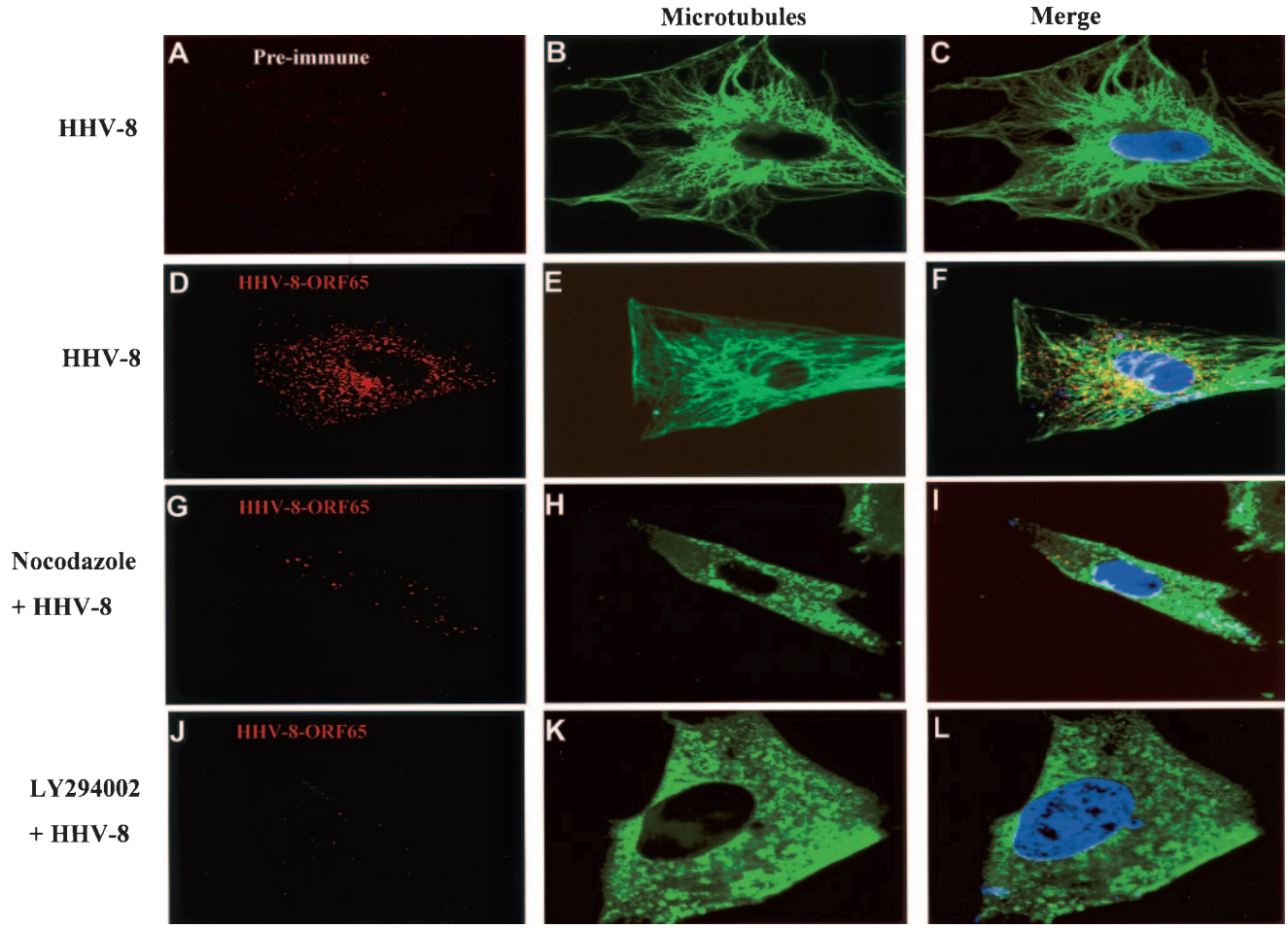

FIG. 9. Confocal microscopic examination of HHV-8 trafficking in the cell cytoplasm. Untreated HFF cells (A to F) or HFF cells preincubated with 10 μg of nocodazole/ml (G to I) or with 50 μM LY294002 (J to L) were infected with HHV-8 at ~50 copies/cell for 1 h at 37°C. The cells were washed, fixed, and permeabilized before being doubly labeled with preimmune IgG antibodies (A) (red), rabbit anti-HHV-8 ORF65 IgG antibodies (D, G, and J) (red), and a MAb against α-tubulin (B, E, H, and K) (green). Nuclei were stained with DAPI (blue). Laser scanning confocal microscopic images were obtained sequentially at a 1-μm thickness, and representative sections shown are through the middle of the cell (10 μm deep). Magnification, ×40.

cient entry of the virus. Since nocodazole does not affect the endosomal pH but inhibits the microtubule-dependent transport of endosomal carrier vesicles to late endosomes (10), MT depolymerization may affect the migration of HHV-8-containing endocytic vesicles. In addition, since MTs may also play important roles in capsid movement after release from the endocytic vesicles, these results suggest that the HHV-8-induced polymerization of MTs plays important roles in the nuclear trafficking of HHV-8. These data clearly demonstrate the importance of the HHV-8-induced signal cascade and the polymerization of MTs in the nuclear trafficking of HHV-8.

Dynein motor function is critical for transport of HHV-8 DNA to the nucleus. Dyneins are large protein complexes that function as MT-based molecular motors generating the driving force towards the minus end of microtubules, with the intermediate and light chains presumably involved in dynein attachment to the appropriate cargo (41). Many viruses sequester the dynein machinery of infected cells to move along the microtubules and gain access to the cell nucleus (24, 47, 62, 69). Since the requirement of intact MTs for the molecular trafficking of HHV-8 became apparent by the results described above, we examined the role of the dynein motor complex in this process.

The cytoplasmic dynein complex associates with a second protein complex called dynactin that contains four molecules of dynamitin among other molecular components (41). The overexpression of dynamitin disrupts the dynactin complex and the dynein motor function (30). To determine the role of dynein motors in HHV-8 nuclear trafficking, we used a p50/dynamitin plasmid expressing c-Myc-tagged p50/dynamitin and enhanced GFP (EGFP) under the control of a cytomegalovirus (CMV) promoter (30). 293 and CV-1 cells were transfected with this plasmid, and about 60 to 70% EGFP-expressing cells were observed under our transfection conditions. The expression of dynamitin was further verified by IFA (Fig. 10A) and immunoblot analysis with antibodies detecting the c-Myc tag (Fig. 10B). These transfected cells were infected with HHV-8 for 3 h, and viral DNA copies associated with the infected cell nuclei were quantified by real-time DNA PCR. Compared to the case for cells carrying a control EGFP vector plasmid, a significant reduction (~50%) in the nuclear trafficking of

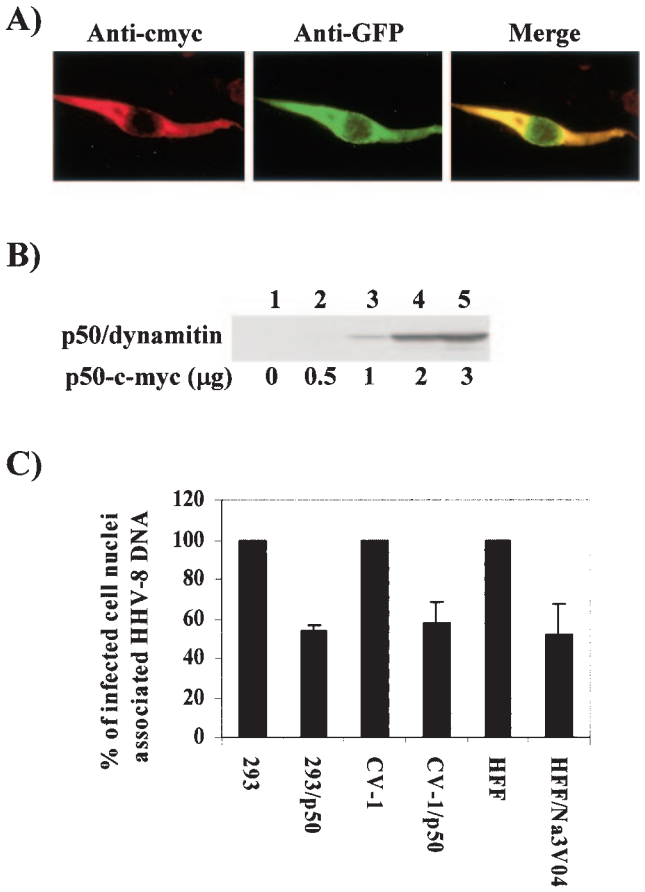

FIG. 10. HHV-8 utilizes the cytoplasmic dynein motors for trafficking into the cell nucleus. (A) Expression of p50/dynamitin in 293 cells. 293 cells were transfected for 8 h with a p50/dynamitin plasmid expressing a c-Myc–p50 fusion protein and an EGFP gene under the control of the CMV promoter. The expression of c-Myc and EGFP was monitored by IFA with MAbs against c-Myc and GFP. (B) Immunoblot detection of p50 expression in cells transfected with different concentrations of a p50/dynamitin–c-Myc-expressing plasmid by the use of anti-c-Myc antibodies. (C) Overexpression of dynamitin inhibiting the dynein motor blocks infected cell nucleus-associated HHV-8 DNA. 293 cells transfected with the pCMV plasmid (293) and the p50–c-Myc plasmid (293/p50), CV-1 cells transfected with the pCMV plasmid (CV-1) and the p50–c-Myc plasmid (CV-1/p50), and HFF cells preincubated with 100 μM Na_3VO_4 or DMEM were infected with HHV-8 for 3 h. The cells were washed to remove the unbound virus, treated with trypsin-EDTA to remove the bound but noninternalized virus, and subjected to estimates of the HHV-8 DNA copy numbers associated with the infected cell nuclei by real-time DNA PCR as described in the legend to Fig. 3. Each reaction was done in duplicate, and each bar represents the mean ± SD for three experiments.

HHV-8 DNA was observed in 293 (293/p50) and CV-1 (CV-1/p50) cells expressing p50/dynamitin (Fig. 10C). Similar amounts of virus binding and internalization were observed in p50/dynamitin-expressing and control cells (data not shown), thus suggesting that the reduction in nucleus-associated HHV-8 DNA copy numbers was not due to reduced HHV-8 binding or internalization. Sodium orthovanadate (Na_3VO_4) is a well-described inhibitor of dynein activity (32, 41). The preincubation of HFF cells with a nontoxic 100 μM concentration of Na_3VO_4 reduced the amount of infected cell nucleus-associated HHV-8 DNA about 45% (Fig. 10C), and the reduction was about 68% at a concentration of 200 μM (data not shown), thus validating the specificity of the above observations. Together, these results strongly demonstrate a role for dynein motors in the cytoplasmic trafficking of HHV-8 and in the delivery of viral DNA to the nucleus.

DISCUSSION

The eukaryotic cytoskeleton comprising MFs, IFs, and MTs performs a broad range of complex cellular activities, such as vesicle and particle movements, cell motility, cell shape determination, and chromosome movement during mitosis (35). Such involvement and its dynamic nature make the cytoskeleton a good target for exploitation by viruses, and many viruses hijack the cytoskeleton to facilitate their movement in the cytoplasm to the nucleus or to the perinuclear virus factories (7, 23, 25, 61, 62, 69). For example, at early times after infection, baculovirus (*Autographa californica*) induces the thick actin bundles to assist with transport of the viral genome into the nucleus (17). Vaccinia virus induces actin polymerization directly behind the virus particle as a means of propelling the virus through the cell (23). Simian virus 40 and polyomavirus require both MF and MT networks for transport to the infected cell nucleus (34, 54), and HIV-1 and HSV-1 associate with the cytoplasmic MT-dependent dynein complex and utilize the MT network for nuclear transport (28, 47). In the present study, we described extensive and thorough analyses of the mechanism of HHV-8 virion transport to the nucleus. These studies are the first report on the exploitation of the cytoskeleton by HHV-8 during its entry into target cells as well as the first report demonstrating the direct role of virus-induced host cell signal pathways in the cytoplasmic transport of viral capsids.

The role of the cytoskeleton in the intracellular transport of viruses has been demonstrated by the physical association of viruses with the cytoskeleton and/or by the use of depolymerizing agents that affect the trafficking of viruses to the nucleus or perinuclear region. The uptake of adenovirus by target cells can be inhibited by a treatment with the MF-depolymerizing agent cyto D (51, 61, 62, 69). Although HHV-8-induced morphological changes such as the formation of actin stress fibers, lamellipodia, and filopodia (50, 60) are suggestive of a modulation of actin MFs, our studies suggest that HHV-8 infection and trafficking do not require intact MFs. In contrast, several lines of evidence, such as the physical association of HHV-8 with the MT network and its abolition by nocodazole, the induction of hyperacetylation to stabilize the MTs, and the significant reduction in HHV-8 DNA associated with infected cell nuclei by MT depolymerization, clearly demonstrated the requirement of an intact MT network for transport of the HHV-8 genome in the cytoplasm. HHV-8 binding and uptake were not affected by MT-depolymerizing drugs, which is not surprising as these drugs do not affect the cell surface expression of cellular proteins (42, 46, 61, 69). Nocodazole and Colcemid disrupt the MT network by inhibiting the polymerization of tubulin monomers (21, 42, 61, 69), and these drugs have been widely used to study the association of viruses with microtubules (15, 34, 61, 69). The presence of glu-tubulin, an MT depolymerization-resistant minor variant of α-tubulin (53),

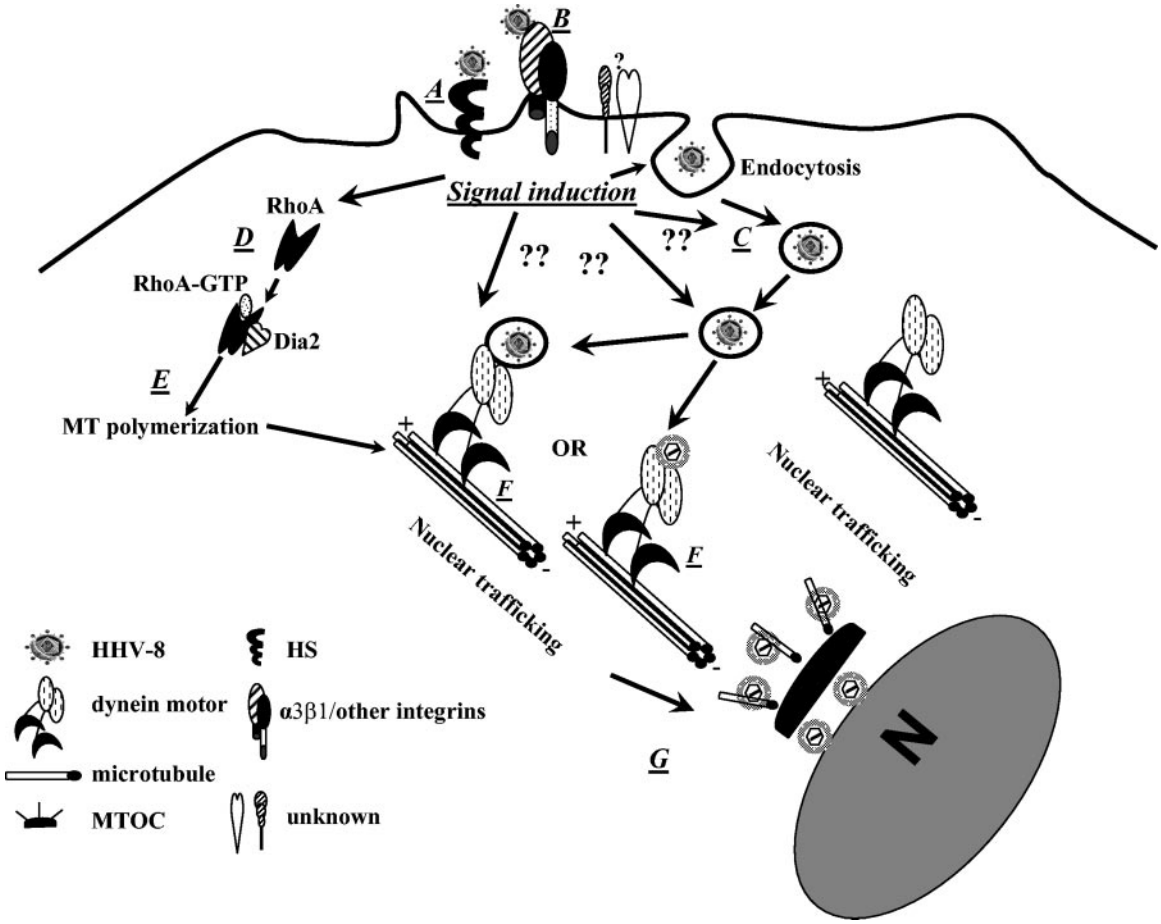

FIG. 11. Model for cytoplasmic transport of HHV-8. After an interaction with cell surface heparan sulfate (HS) (A), integrin α3β1, and another unknown receptor(s), HHV-8 is taken into an endocytic vesicle (C). The interaction of the virus-receptor complex triggers signaling (D). Rho GTPases are some of the downstream mediators of the induced signaling pathways, which facilitate virus movement by inducing MT stabilization and regulating MT dynamics (E). The endocytic vesicles with virus or released capsid/tegument complexes bind to dynein motor components (F), are transported along the MTs to reach the MTOC (G) near the nuclear vicinity, and deliver the viral DNA into the nucleus. The question marks indicate the potential stages of HHV-8 entry and infection at which the induced signaling events may have a role based on the known functions of these signaling events.

may be one of the reasons for the incomplete inhibition of HHV-8 nuclear trafficking by nocodazole and Colcemid.

The MT network, which plays a critical role in the nuclear trafficking of HHV-8, is a dynamic and polarized structure. Relatively stable minus ends are localized to the MTOC, which is typically located at the perinuclear position in cultured cells. Directional movement along MTs is mediated by motor proteins, which hydrolyze ATP to induce conformational changes in their structure. The dynamic, fast-growing, and fast-shrinking plus ends extend toward the cell periphery, and kinesin superfamily motors typically move toward the MT plus ends (24, 46, 47, 62–65). The dynein motors mediate minus-end-directed movement towards the nucleus, and adenoviruses and HSV-1 utilize the dynein motors and MTs for the transport of capsids in the cytoplasm (28). Similarly, HHV-8 utilizes the dynein motors to facilitate movement, as shown by a reduction in HHV-8 nuclear trafficking by the overexpression of dynamitin, which inhibits dynein-dynactin complex formation, and by Na_3VO4. HSV-1 VP22 induces the aggregation of MTs and interacts with the intermediate chain of cytoplasmic dynein via its UL34 protein (70). Incoming nucleocapsids of pseudorabies virus, an alphaherpesvirus that is closely related to HSV-1, were also shown to be associated with MTs and to utilize them for movement to the nucleus (38). This interaction is believed to be mediated by the PRV UL25 protein, a minor but essential component of the capsid, which colocalizes with MTs and accumulates at the MTOC (38). Whether HHV-8 encodes a protein(s) that physically associates with the MT motor and aids in the movement of cargo along the MT network is not currently known and needs to be investigated.

The utilization of the MT network by HHV-8 is not a unique observation, as other viruses have been shown to require the MF or MT cytoskeleton. However, this is the first demonstration of a direct role for the signal cascade induced by a virus in cytoplasmic trafficking. The complex signaling events associated with internalization of the bound virus and trafficking of the internalized capsid remain largely unknown. The well-studied adenovirus (Ad) types 2 and 5 bind to a primary receptor, the coxsackie virus and adenovirus receptor. Coxsackie virus and adenovirus receptor-docked particles activate the integrin

coreceptors, which triggers a variety of cell responses, including endocytosis and macropinocytosis (51, 62). A major question arising from Ad entry studies is whether integrins promote virus entry and infection via specific cell signaling events. Similar to our results with HHV-8, adenoviruses induce the ERK1/2 mitogen-activated protein (MAP) kinases via the integrin-dependent focal adhesion kinase (pp125FAK) (51). FAK activation appears to play little role in integrin-mediated Ad endocytosis since the virus infected FAK null Du3 mouse fibroblast cells with a similar efficiency as that for parental $FAK^{+/+}$ Du17 cells (51). This is in contrast to HHV-8, whose infection efficiency is severely impaired in FAK null Du3 cells (50). Adenovirus internalization was shown to be regulated by the PI-3K and p130CAS proteins (51). Pharmacologic inhibitors of PI-3K but not of ERK MAP kinases inhibited Ad internalization and infection (51). Similar to the results of our study, the entry of adenoviruses was also negatively regulated when Rho GTPases were inhibited or when dominant-negative mutants of Rac and Cdc42 were overexpressed (51). The postentry trafficking of adenovirus capsids activates the protein kinase A and p38/MAPK pathways, and such activation appears to enhance the minus-end-directed transport of adenovirus on MTs (65). However, how adenovirus-induced Rho GTPase and other signaling pathways aid in transport in the cytoplasm is not fully understood.

The cytoskeletal MFs, MTs, and IFs are highly dynamic structures that cooperate in response to extracellular stimuli and allow the cell to modulate its shape, to migrate, and to divide. The Rho GTPases are tightly involved in the coordination of these networks, and RhoA, Rac, and Cdc42 are best known for regulating the actin cytoskeleton (52). However, only very recently have studies begun to dissect out the role of Rho GTPases and their effector molecules in the modulation of cytoskeletal elements. Emerging evidence clearly demonstrates the influence exerted by the Rho GTPases over the MTs and thus links the Rho GTPases to MT dynamics (22, 37). Moreover, studies also demonstrate that MTs themselves can influence Rho GTPases (27, 33, 68). Growing MTs target Rho-dependent focal adhesions and regulate their turnover (39). Active RhoA stabilizes a subset of MTs (22, 53), while activated Rac binds tubulin (12) and is associated with the recovery of fibroblasts from nocodazole treatment (68). How HHV-8-induced signaling pathways contribute to the acetylation of MTs is not known at present. However, evidence such as the inhibition of HHV-8-induced hyperacetylation and the stabilization of MTs by the Rho GTPase inhibitor CdTxB, the significant increase in HHV-8 nuclear trafficking by the Rho GTPase agonist CNF-1, and its significant decrease by the antagonist CdTxB suggest that Rho GTPases have profound control over HHV-8-induced MT polymerization. Together with the activation of RhoA-dependent diaphanous 2, one of the various signaling molecules associated with Rho GTPases and MT polymerization, these results demonstrate that HHV-8–integrin interaction-dependent signaling pathways induce MT polymerization and show evidence for the first time for a virus infection that MT dynamics are controlled by Rho GTPases. Whether HHV-8-induced signaling pathways play a role in dynein motor movement is not known at present and needs to be explored.

MTs and their motors are also known to have roles in endocytic regulation (10). Adenovirus capsid movement towards the nucleus is dependent both on endocytic trafficking and on the MT network (65). Since HHV-8 enters HFF, 293, and BJAB cells via endocytosis (6, 36) and since microtubules are critical for the transport of endosomal carrier vesicles to late endosomes (8, 10, 19), it is reasonable to assume that the role of MTs in HHV-8 trafficking may also be at the stage of transport from early to late endosomes (8, 10, 19). In this regard, it is interesting that recent studies have uncovered a multitude of control points for Rho GTPases in the endocytic pathways and an intimate connection between these signaling proteins and intracellular traffic (56). The activated Rac, Rho, Cdc42, and Rab5 GTPases act as molecular switches in various signal transduction pathways and are essential for the modulation of actin dynamics, the formation of endocytic vesicles, their fission, cytoskeletal transport, endosome movement, the fusion of endocytic vesicles, and recycling (56).

HHV-8 and HHV-8 gB interactions with integrin, the induction of FAK–Src–PI-3K, the upstream mediator of Rho GTPases, the activation of RhoA, and the associated diaphanous 2 protein required for microtubular stabilization and for regulation of the movement of endocytic vesicles suggest that HHV-8 manipulates signaling pathways, resulting in aid in the movement of its capsid or tegument in the cytoplasm. Our data demonstrate a link between HHV-8-induced signaling pathways and MT network dynamics, which together with the dynein motor complex collectively facilitate the cytoplasmic transport of HHV-8 (Fig. 11). Thus, our findings further support our earlier suggestion (5, 50) that besides providing a conduit for the entry of the viral genome into the interior of cells, the interactions of HHV-8 with integrins and other host cell surface molecules and the accompanying preexisting host cell signaling cascades have an active role in virus entry, transport of the viral genome to the nucleus, and the establishment of a successful infection. The results presented here will lead to further exploration of the dynamic interactions of HHV-8 with the various components of cytoskeletal and signaling pathways during entry and infection, which may lead to the development of novel strategies to block the establishment of target cell infection by HHV-8.

ACKNOWLEDGMENTS

This study was supported in part by Public Health Service grants CA 75911 and CA 099925 to B.C. and by a University of Kansas Medical Center Biomedical Research Training Program postdoctoral fellowship to P.P.N.

We thank Ling Zeng for technical assistance. We thank Jeffrey Vieira (Fred Hutchinson Cancer Research Center, Seattle, Wash.) for kindly providing the GFP–HHV-8 (rKSHV.152)-harboring BCBL-1 cells. We thank Gudula Schmidt (Universitat Freiburg) for *E. coli* CNF-1, Andre Sobel (Inserm, Paris, France) for antibodies against stathmin and pSer16-stathmin, Richard Vallee (Columbia University) for the p50/dynamitin construct, and Elizabeth Petroske of the Confocal Imaging Center at the University of Kansas Medical Center for confocal image acquisition.

REFERENCES

1. **Aktories, K., G. Schmidt, and I. Just.** 2000. Rho GTPases as targets of bacterial protein toxins. J. Biol. Chem. **381:**421–426.
2. **Aktories, K., and G. Schmidt.** 2003. A new turn in Rho GTPase activation by *Escherichia coli* cytotoxic necrotizing factors. Trends Microbiol. **11:**152–155.
3. **Akula, S. M., F. Z. Wang, J. Vieira, and B. Chandran.** 2001. Human herpesvirus 8 interaction with target cells involves heparan sulfate. Virology **282:**245–255.

4. **Akula, S. M., N. P. Pramod, F. Z. Wang, and B. Chandran.** 2001. Human herpesvirus 8 envelope-associated glycoprotein B interacts with heparan sulfate-like moieties. Virology **284:**235–249.
5. **Akula, S. M., N. P. Pramod, F. Z. Wang, and B. Chandran.** 2002. Integrin α3β1 (CD49c/28) is a cellular receptor for Kaposi's sarcoma associated herpesvirus (KSHV/HHV-8) entry into the target cells. Cell **108:**407–419.
6. **Akula, S. M., P. P. Naranatt, N. S. Walia, F. Z. Wang, B. Fegley, and B. Chandran.** 2003. Kaposi's sarcoma-associated herpesvirus (human herpesvirus 8) infection of human fibroblast cells occurs through endocytosis. J. Virol. **77:**7978–7990.
7. **Alonso, C., J. Miskin, B. Hernaez, P. Fernandez-Zapatero, L. Soto, C. Canto, I. Rodriguez-Crespo, L. Dixon, and J. M. Escribano.** 2001. African swine fever virus protein p54 interacts with the microtubular motor complex through direct binding to light-chain dynein. J. Virol. **75:**9819–9827.
8. **Aniento, F., N. Emans, G. Griffiths, and J. Gruenberg.** 1993. Cytoplasmic dynein-dependent vesicular transport from early to late endosomes. J. Cell Biol. **123:**1373–1387.
9. **Antman, K., and Y. Chang.** 2000. Kaposi's sarcoma. N. Engl. J. Med. **342:** 1027–1038.
10. **Apodaca, G.** 2001. Endocytic traffic in polarized epithelial cells: role of the actin and microtubule cytoskeleton. Traffic **2:**149–159.
11. **Bechtel, J. T., Y. Liang, J. Hvidding, and D. Ganem.** 2003. Host range of Kaposi's sarcoma-associated herpesvirus in cultured cells. J. Virol. **77:**6474–6481.
12. **Best, A., S. Ahmed, R. Kozma, and L. Lim.** 1996. The Ras-related GTPase Rac1 binds tubulin. J. Biol. Chem. **271:**3756–3762.
13. **Bishop, A., and A. Hall.** 2000. Rho GTPases and their effector proteins. Biochem. J. **348:**241–255.
14. **Campbell, E. M., and T. J. Hope.** 2003. Role of the cytoskeleton in nuclear import. Adv. Drug Deliv. Rev. **55:**761–771.
15. **Candurra, N. A., M. J. Lago, L. Maskin, and E. B. Damonte.** 1999. Involvement of the cytoskeleton in Junin virus multiplication. J. Gen. Virol. **80:**147–156.
16. **Chang, Y., E. Cesarman, M. S. Pessin, F. Lee, J. Culpepper, D. M. Knowles, and P. S. Moore.** 1994. Identification of herpesvirus-like DNA sequences in AIDS-associated Kaposi's sarcoma. Science **266:**1865–1869.
17. **Charlton, C. A., and L. E. Volkman.** 1993. Penetration of Autographa californica nuclear polyhedrosis virus nucleocapsids into IPLB Sf 21 cells induces actin cable formation. Virology **197:**245–254.
18. **Chaves-Olarte, E., P. Low, E. Freer, T. Norlin, M. Weidmann, C. von Eichel-Streiber, and M. Thelestam.** 1999. A novel cytotoxin from Clostridium difficile serogroup F is a functional hybrid between two other large clostridial cytotoxins. J. Biol. Chem. **274:**11046–11052.
19. **Clague, M. J., S. Urbe, F. Aniento, and J. Gruenberg.** 1994. Vacuolar ATPase activity is required for endosomal carrier vesicle formation. J. Biol. Chem. **269:**21–24.
20. **Clark, E. A., and J. S. Brugge.** 1995. Integrins and signal transduction pathways: the road taken. Science **268:**233–239.
21. **Cleveland, D. W., M. A. Lopata, P. Sherline, and M. W. Kirschner.** 1981. Unpolymerized tubulin modulates the level of tubulin mRNAs. Cell **25:**537–546.
22. **Cook, T. A., T. Nagasaki, and G. G. Gundersen.** 1998. Rho guanosine triphosphatase mediates the selective stabilization of microtubules induced by lysophosphatidic acid. J. Cell Biol. **141:**175–185.
23. **Cudmore, S., I. Reckmann, G. Griffiths, and M. Way.** 1996. Vaccinia virus: a model system for actin-membrane interactions. J. Cell Sci. **109:**1739–1747.
24. **Cullen, B. R.** 2001. Journey to the center of the cell. Cell **105:**697–700.
25. **Dales, S., and Y. Chardonnet.** 1973. Early events in the interaction of adenoviruses with HeLa cells. IV. Association with microtubules and the nuclear pore complex during vectorial movement of the inoculum. Virology **56:**465–483.
26. **Damiani, M. T., and M. I. Colombo.** 2003. Microfilaments and microtubules regulate recycling from phagosomes. Exp. Cell Res. **289:**152–161.
27. **Daub, H., K. Gevaert, J. Vandekerckhove, A. Sobel, and A. Hall.** 2001. Rac/Cdc42 and p65PAK regulate the microtubule-destabilizing protein stathmin through phosphorylation at serine 16. J. Biol Chem. **276:**1677–1680.
28. **Dohner, K., A. Wolfstein, U. Prank, C. Echeverri, D. Dujardin, R. Vallee, and B. Sodeik.** 2002. Function of dynein and dynactin in herpes simplex virus capsid transport. Mol. Biol. Cell **13:**2795–2809.
29. **Dramsi, S., and P. Cossart.** 1998. Intracellular pathogens and the actin cytoskeleton. Annu. Rev. Cell Dev. Biol. **14:**137–166.
30. **Echeverri, C. J., B. M. Paschal, K. T. Vaughan, and R. B. Vallee.** 1996. Molecular characterization of the 50-kD subunit of dynactin reveals function for the complex in chromosome alignment and spindle organization during mitosis. J. Cell Biol. **132:**617–633.
31. **Elliott, G., and P. O'Hare.** 1998. Herpes simplex virus type 1 tegument protein VP22 induces the stabilization and hyperacetylation of microtubules. J. Virol. **72:**6448–6455.
32. **Finley, B. B., S. Ruschkowski, and S. Dedhar.** 1991. Cytoskeletal rearrangements accompanying Salmonella entry into epithelial cells. J. Cell Sci. **99:** 283–296.
33. **Fukata, M., T. Watanabe, J. Noritake, M. Nakagawa, M. Yamaga, S. Kuroda, Y. Matsuura, A. Iwamatsu, F. Perez, and K. Kaibuchi.** 2002. Rac1 and Cdc42 capture microtubules through IQGAP1 and CLIP-170. Cell **109:**873–885.
34. **Gilbert, J. M., I. G. Goldberg, and T. L. Benjamin.** 2003. Cell penetration and trafficking of polyomavirus. J. Virol. **77:**2615–2622.
35. **Goodson, H. V., C. Valetti, and T. E. Kreis.** 1997. Motors and membrane traffic. Curr. Opin. Cell Biol. **9:**18–28.
36. **Inoue, N., J. Winter, R. B. Lal, M. K. Offermann, and S. Koyano.** 2003. Characterization of entry mechanisms of human herpesvirus 8 by using an Rta-dependent reporter cell line. J. Virol. **77:**8147–8152.
37. **Ishizaki, T., Y. Morishima, M. Okamoto, T. Furuyashiki, T. Kato, and S. Narumiya.** 2001. Coordination of microtubules and the actin cytoskeleton by the Rho effector mDia1. Nat. Cell Biol. **3:**8–14.
38. **Kaelin, K., S. Dezelee, M. J. Masse, F. Bras, and A. Flamand.** 2000. The UL25 protein of pseudorabies virus associates with capsids and localizes to the nucleus and to microtubules. J. Virol. **74:**474–482.
39. **Kaverina, I., K. Rottner, and J. V. Small.** 1998. Targeting, capture, and stabilization of MTs at early focal adhesions. J. Cell Biol. **142:**181–190.
40. **Kazmierczak, B. I., T. S. Jou, K. Mostov, and J. N. Engel.** 2001. Rho GTPase activity modulates *Pseudomonas aeruginosa* internalization by epithelial cells. Cell Microbiol. **3:**85–98.
41. **King, S. M.** 2000. The dynein microtubule motor. Biochim. Biophys. Acta **1496:**60–75.
42. **Kizhatil, K., and L. M. Albritton.** 1997. Requirements for different components of the host cell cytoskeleton distinguish ecotropic murine leukemia virus entry via endocytosis from entry via surface fusion. J. Virol. **71:**7145–7156.
43. **Krishnan, H. H., P. P. Naranatt, M. S. Smith, L. Zeng, C. Bloomer, and B. Chandran.** 2004. Concurrent expression of latent and a limited number of lytic genes with immune modulation and anti-apoptotic functions by Kaposi's sarcoma-associated herpesvirus early during infection of primary endothelial and fibroblast cells and subsequent decline of lytic gene expression. J. Virol. **78:**3601–3620.
44. **Kristensson, K., E. Lycke, M. Roytta, B. Svennerholm, and A. Vahlne.** 1986. Neuritic transport of herpes simplex virus in rat sensory neurons in vitro. Effects of substances interacting with microtubular function and axonal flow [nocodazole, taxol and erythro-9-3-(2-hydroxynonyl) adenine]. J. Gen. Virol. **67:**2023–2028.
45. **Lo, P., X. Yu, I. Atanasov, B. Chandran, and Z. H. Zhou.** 2003. Three-dimensional localization of pORF65 in Kaposi's sarcoma-associated herpesvirus capsid. J. Virol. **77:**4291–4297.
46. **Mandelkow, E., and E. M. Mandelkow.** 1995. Microtubules and microtubule-associated proteins. Curr. Opin. Cell Biol. **7:**72–81.
47. **McDonald, D., M. A. Vodicka, G. Lucero, T. M. Svitkina, G. G. Borisy, M. Emerman, and T. J. Hope.** 2002. Visualization of the intracellular behavior of HIV in living cells. J. Cell Biol. **159:**441–452.
48. **Naranatt, P. P., H. H. Krishnan, S. R. Svojanovsky, C. Bloomer, S. Mathur, and B. Chandran.** 2004. Host gene induction and transcriptional reprogramming in Kaposi's-sarcoma associated herpesvirus (KSHV/HHV-8) infected endothelial, fibroblast and B cells: insights into modulation events early during infection. Cancer Res. **64:**72–84.
49. **Naranatt, P. P., S. M. Akula, and B. Chandran.** 2002. Characterization of gamma 2-human herpesvirus-8 glycoproteins gH and gL. Arch. Virol. **147:** 1349–1370.
50. **Naranatt, P. P., S. M. Akula, C. A. Zien, H. H. Krishnan, and B. Chandran.** 2003. Kaposi's sarcoma-associated herpesvirus induces the phosphatidylinositol 3-kinase–PKC-zeta–MEK–ERK signaling pathway in target cells early during infection: implications for infectivity. J. Virol. **77:**1524–1539.
51. **Nemerow, G. R.** 2000. Cell receptors involved in adenovirus entry. Virology **274:**1–4.
52. **Nobes, C. D., and A. Hall.** 1995. Rho, Rac, and Cdc42 GTPases regulate the assembly of multimolecular focal complexes associated with actin stress fibers, lamellipodia, and filopodia. Cell **81:**53–62.
53. **Palazzo, A. F., T. A. Cook, A. S. Alberts, and G. G. Gundersen.** 2001. mDia mediates Rho-regulated formation and orientation of stable microtubules. Nat. Cell Biol. **3:**723–729.
54. **Pelkmans, L., D. Puntener, and A. Helenius.** 2002. Local actin polymerization and dynamin recruitment in SV40-induced internalization of caveolae. Science **296:**535–539.
55. **Piperno, G., M. LeDizet, and X. J. Chang.** 1987. Microtubules containing acetylated alpha-tubulin in mammalian cells in culture. J. Cell Biol. **104:**289–302.
56. **Qualmann, B., and H. Mellor.** 2003. Regulation of endocytic traffic by Rho GTPases. Biochem. J. **371:**233–241.
57. **Renne, R., D. Blackbourn, D. Whitby, J. Levy, and D. Ganem.** 1998. Limited transmission of Kaposi's sarcoma-associated herpesvirus in cultured cells. J. Virol. **72:**5182–5188.
58. **Schulz, T. F., Y. Chang, and P. S. Moore.** 1998. Kaposi's sarcoma-associated herpesvirus (human herpesvirus 8), p. 87–134. *In* D. J. McCance (ed.), Human tumor viruses. American Society for Microbiology, Washington, D.C.
59. **Seksek, O., J. Biwersi, and A. S. Verkman.** 1997. Translational diffusion of

macromolecule-sized solutes in cytoplasm and nucleus. J. Cell Biol. **138:**131–142.
60. **Sharma-Walia, N., P. P. Naranatt, H. H. Krishnan, L. Zeng, and B. Chandran.** 2004. Kaposi's sarcoma associated herpesvirus envelope glycoprotein gB induces the integrin-dependent focal adhesion kinase-Src-PI-3K-RhoGTPase signal pathways and cytoskeletal rearrangements. J. Virol. **78:** 4207–4223.
61. **Sieczkarski, S. B., and G. R. Whittaker.** 2002. Dissecting virus entry via endocytosis. J. Gen. Virol. **83:**1535–1545.
62. **Sodeik, B.** 2000. Mechanisms of viral transport in the cytoplasm. Trends Microbiol. **8:**465–472.
63. **Stidwell, R. P., and U. F. Greber.** 2000. Intracellular virus trafficking reveals physiological characteristics of cytoskeleton. News Physiol. Sci. **15:**67–71.
64. **Suomalainen, M., M. Y. Nakano, S. Keller, K. Boucke, R. P. Stidwill, and U. F. Greber.** 1999. Microtubule-dependent plus- and minus end-directed motilities are competing processes for nuclear targeting of adenovirus. J. Cell Biol. **144:**657–672.
65. **Suomalainen, M., M. Y. Nakano, K. Boucke, S. Keller, and U. F. Greber.** 2001. Adenovirus-activated PKA and p38/MAPK pathways boost microtubule-mediated nuclear targeting of virus. EMBO J. **20:**1310–1319.
66. **Vieira, J., P. O'Hearn, L. Kimball, B. Chandran, and L. Corey.** 2001. Activation of Kaposi's sarcoma-associated herpesvirus (human herpesvirus 8) lytic replication by human cytomegalovirus. J. Virol. **75:**1378–1386.
67. **Wang, F. Z., S. M. Akula, N. P. Pramod, L. Zeng, and B. Chandran.** 2001. Human herpesvirus 8 envelope glycoprotein K8.1A interaction with the target cells involves heparan sulfate. J. Virol. **75:**7517–7527.
68. **Waterman-Storer, C. M., R. A. Worthylake, B. P. Liu, K. Burridge, and E. D. Salmon.** 1999. Microtubule growth activates Rac1 to promote lamellipodial protrusion in fibroblasts. Nat. Cell Biol. **1:**45–50.
69. **Whittaker, G. R., M. Kann, and A. Helenius.** 2000. Viral entry into the nucleus. Annu. Rev. Cell Dev. Biol. **16:**627–651.
70. **Ye, G. J., K. T. Vaughan, R. B. Vallee, and B. Roizman.** 2000. The herpes simplex virus 1 UL 34 protein interacts with a cytoplasmic dynein intermediate chain and targets nuclear membrane. J. Virol. **74:**1355–1363.